Liquid-gas phase transition in canonical and micro-canonical ensembles of strange hadronic matter

K. Miyazaki

E-mail: miyazakiro@rio.odn.ne.jp

Abstract

New calculus of the liquid-gas phase transition is developed for the strange hadronic matter in the relativistic mean-field model. Against the familiar geometrical construction of phase equilibrium we investigate canonical and micro-canonical ensembles. For the former the pressure and the chemical potentials are determined from definite values of baryon density, strangeness and temperature. We recover the convex minimized Helmholtz energy. Due to the field-dependent meson-nucleon coupling constants, the section of binodal surface has no critical point. The appearance of the retrograde condensation is also proved. For micro-canonical ensemble the temperature and the chemical potentials are determined from definite values of baryon density, strangeness and pressure. We recover the concave maximized entropy and the minimized Gibbs energy. The resultant caloric and boiling curves are analyzed. Because the derivatives of chemical potentials have discontinuities at transition points, we conclude against the preceding works that the phase transition is the first order.

1 Introduction

The author has recently developed a new calculus [1,2] of the liquid-gas phase transition [3-6] in asymmetric nuclear matter against the geometrical construction used widely in the literature [7-11]. The asymmetric nuclear matter is a binary system that has two independent chemical potentials of proton and neutron. According to the Gibbs condition on phase equilibrium, both the chemical potentials in liquid and gaseous phases are equilibrated. In the geometrical construction the chemical potentials are determined for definite values of temperature, pressure and the asymmetry of nuclear matter. To the contrary, our calculus is applicable to canonical [1] and micro-canonical ensembles [2] of nuclear matter.

The strange hadronic matter (SHM) [12-18] composed of nucleons and hyperons is another binary system in nuclear physics. It has two independent chemical potentials [15], the baryon and strangeness chemical potentials. The liquid-gas phase transition in

SHM has been also investigated [19-22] in terms of the geometrical construction. To the contrary, in the present paper we apply the calculus in Refs. [1] and [2] to the liquid-gas phase transition in canonical and micro-canonical ensembles of SHM. We are based on the relativistic mean-field (RMF) model of SHM developed in Ref. [18]. The model has field-dependent meson-baryon coupling constants from a constituent quark picture of baryons. The hidden strange mesons σ^* and ϕ [12] are taken into account.

2 Maxwell construction of phase transition

At finite temperature T the thermodynamic potential per volume $\tilde{\Omega} \equiv \Omega/V$ of SHM is

$$\begin{aligned}\tilde{\Omega} &= \frac{1}{2}\, m_\sigma^2 \left\langle \sigma \right\rangle^2 - \frac{1}{2}\, m_\omega^2 \left\langle \omega_0 \right\rangle^2 + \frac{1}{2}\, m_{\sigma^*}^2 \left\langle \sigma^* \right\rangle^2 - \frac{1}{2}\, m_\phi^2 \left\langle \phi_0 \right\rangle^2 \\ &\quad - T \sum_{B=N,\Lambda,\Sigma,\Xi} \gamma_B \int_0^\infty \frac{d^3\mathbf{k}}{(2\pi)^3} \left\{ \ln\left[1+\exp\left(\frac{\nu_B - E_{kB}^*}{T}\right)\right] \right. \\ &\qquad \left. + \ln\left[1+\exp\left(\frac{-\nu_B - E_{kB}^*}{T}\right)\right] \right\}, \end{aligned} \tag{1}$$

where $M_B^* = m_B^* M_B$ and $E_{kB}^* = (\mathbf{k}^2 + M_B^{*\,2})^{1/2}$ are the effective mass and the energy of each baryon in SHM. In the present paper we set the Boltzmann constant as a unit. The spin-isospin degeneracy factor is defined as $\gamma_B = \{4, 2, 6, 4\}$ for $B = \{N, \Lambda, \Sigma, \Xi\}$. The ν_B is given by the chemical potential μ_B and the vector potential V_B of each baryon as

$$\nu_B = \mu_B - V_B. \tag{2}$$

Because of the chemical equilibrium condition [15]

$$\mu_\Lambda = \mu_\Sigma = \frac{\mu_N + \mu_\Xi}{2}, \tag{3}$$

we have two independent chemical potentials μ_N and μ_Λ or the strangeness chemical potential [15] $\mu_S = \mu_N - \mu_\Lambda$.

Then, the effective masses m_N^* and m_Λ^* and the vector potential V_N and V_Λ are determined from extremizing the thermodynamic potential $\tilde{\Omega}$. The resultant equations are

$$\rho_{bN} + \sum_{Y=\Sigma,\Xi} \left(\frac{g_{YY\omega}^*}{g_{NN\omega}^*} - \frac{g_{YY\phi}^*}{g_{\Lambda\Lambda\phi}^*}\, \frac{g_{\Lambda\Lambda\omega}^*}{g_{NN\omega}^*} \right) \rho_{bY} - \left(\frac{m_\omega}{g_{NN\omega}^*} \right)^2 V_N + \left(\frac{m_\phi}{g_{\Lambda\Lambda\phi}^*} \right)^2 \frac{g_{\Lambda\Lambda\omega}^*}{g_{NN\omega}^*}\, C_{N\Lambda\,\omega} = 0, \tag{4}$$

$$\rho_{b\Lambda} + \sum_{Y=\Sigma,\Xi} \frac{g_{YY\phi}^*}{g_{\Lambda\Lambda\phi}^*}\, \rho_{bY} - \left(\frac{m_\phi}{g_{\Lambda\Lambda\phi}^*} \right)^2 C_{N\Lambda\,\omega} = 0, \tag{5}$$

$$\sum_{B=N,\Sigma,\Xi} \frac{\partial m_B^*}{\partial m_N^*} M_B \rho_{sB} + \sum_{Y=\Sigma,\Xi} \frac{\partial V_Y}{\partial m_N^*} \rho_{bY} + m_\sigma^2 \langle\sigma\rangle \frac{\partial \langle\sigma\rangle}{\partial m_N^*} + m_{\sigma^*}^2 \langle\sigma^*\rangle \frac{\partial \langle\sigma^*\rangle}{\partial m_N^*}$$
$$+ \left(\frac{m_\omega}{g_{NN\omega}^*}\right)^2 \frac{1}{g_{NN\omega}^*} \frac{\partial g_{NN\omega}^*}{\partial m_N^*} V_N^2 + \left(\frac{m_\phi}{g_{\Lambda\Lambda\phi}^*}\right)^2 \frac{1}{g_{\Lambda\Lambda\phi}^*} \frac{\partial g_{\Lambda\Lambda\phi}^*}{\partial m_N^*} C_{N\Lambda\,\omega}^2$$
$$+ \left(\frac{m_\phi}{g_{\Lambda\Lambda\phi}^*}\right)^2 \frac{1}{g_{NN\omega}^*} \left(\frac{\partial g_{\Lambda\Lambda\omega}^*}{\partial m_N^*} - \frac{g_{\Lambda\Lambda\omega}^*}{g_{NN\omega}^*} \frac{\partial g_{NN\omega}^*}{\partial m_N^*}\right) V_N\, C_{N\Lambda\,\omega} = 0, \tag{6}$$

$$\sum_Y \frac{\partial m_Y^*}{\partial m_\Lambda^*} M_Y \rho_{sY} + \sum_{Y=\Sigma,\Xi} \frac{\partial V_Y}{\partial m_\Lambda^*} \rho_{bY} + m_{\sigma^*}^2 \langle\sigma^*\rangle \frac{\partial \langle\sigma^*\rangle}{\partial m_\Lambda^*}$$
$$+ \left(\frac{m_\phi}{g_{\Lambda\Lambda\phi}^*}\right)^2 \frac{1}{g_{NN\omega}^*} \frac{\partial g_{\Lambda\Lambda\omega}^*}{\partial m_\Lambda^*} V_N\, C_{N\Lambda\,\omega} + \left(\frac{m_\phi}{g_{\Lambda\Lambda\phi}^*}\right)^2 \frac{1}{g_{\Lambda\Lambda\phi}^*} \frac{\partial g_{\Lambda\Lambda\phi}^*}{\partial m_\Lambda^*} C_{N\Lambda\,\omega}^2 = 0, \tag{7}$$

where

$$C_{N\Lambda\,\omega} = V_\Lambda - \frac{g_{\Lambda\Lambda\omega}^*}{g_{NN\omega}^*} V_N. \tag{8}$$

The effective masses and the vector potentials of Σ and Ξ are expressed [18] in terms of those of N and Λ. The mean-fields and the effective coupling constants are also expressed [18] in terms of them. In the present paper we use the same meson-baryon coupling constants as EZM-P in Ref. [23].

The baryon and scalar densities in Eqs. (4)-(7) are defined by

$$\rho_{bB} = \gamma_B \int_0^\infty \frac{d^3\mathbf{k}}{(2\pi)^3} \left[n_{kB}\left(m_B^*, v_B; \mu_B, T\right) - \bar{n}_{kB}\left(m_B^*, v_B; \mu_B, T\right)\right], \tag{9}$$

$$\rho_{sB} = \gamma_B \int_0^\infty \frac{d^3\mathbf{k}}{(2\pi)^3} \frac{M_B^*}{E_{kB}^*} \left[n_{kB}\left(m_B^*, v_B; \mu_B, T\right) + \bar{n}_{kB}\left(m_B^*, v_B; \mu_B, T\right)\right], \tag{10}$$

where the Fermi-Dirac distribution functions of each baryon and antibaryon are

$$n_{kB}\left(m_B^*, v_B; \mu_B, T\right) = \left[1 + \exp\left(\frac{E_{kB}^* - \nu_B}{T}\right)\right]^{-1}, \tag{11}$$

$$\bar{n}_{kB}\left(m_B^*, v_B; \mu_B, T\right) = \left[1 + \exp\left(\frac{E_{kB}^* + \nu_B}{T}\right)\right]^{-1}. \tag{12}$$

In our calculations the Fermi integrals are performed using the adaptive automatic integration with 20-points Gaussian quadrature.

For the canonical ensemble of a constant temperature T, a given total baryon density

$$\rho_T = \sum_{B=N,\Lambda,\Sigma,\Xi} \rho_{bB} \tag{13}$$

and a definite strangeness fraction

$$f_S = \frac{\rho_{b\Lambda} + \rho_{b\Sigma} + 2\rho_{b\Xi}}{\rho_T}, \tag{14}$$

we have to solve the 6th-rank simultaneous nonlinear equations (4)-(7), (13) and (14) so that the effective masses m_N^* and m_Λ^*, the vector potentials V_N and V_Λ, and the chemical potentials μ_N and μ_Λ are determined selfconsistently. Using the results, the pressure is calculated from

$$\begin{aligned} P &= \frac{1}{6\pi^2} \sum_{B=N,\Lambda,\Sigma,\Xi} \gamma_B \int_0^\infty dk \, \frac{k^4}{E_{kB}^*} \left[n_{kB}\left(m_B^*, v_B; \mu_B, T\right) + \bar{n}_{kB}\left(m_B^*, v_B; \mu_B, T\right) \right] \\ &\quad - \frac{1}{2} m_\sigma^2 \langle\sigma\rangle^2 + \frac{1}{2} m_\omega^2 \langle\omega_0\rangle^2 - \frac{1}{2} m_{\sigma^*}^2 \langle\sigma^*\rangle^2 + \frac{1}{2} m_\phi^2 \langle\phi_0\rangle^2 . \end{aligned} \tag{15}$$

The black curve in Fig. 1 shows an isotherm of $T = 10$MeV in the pressure-density plane of $f_S = 0.5$. It exhibits typical nature of van der Waals equation of state. The black curve in Fig. 2 shows the corresponding Helmholtz energy per baryon $F/A = G/A - P/\rho_T$ as a function of volume, where $G/A = (\sum_B \mu_B \rho_{bB})/\rho_T$ is the Gibbs energy per baryon. A concave on the curve between $\rho_B^{-1} = 5.74\text{fm}^3$ and 62.73fm^3 marked by the red crosses is a signal of liquid-gas phase transition. Because the Helmholtz energy must be convex, the concave is not realized physically. Although the SHM is a binary system, we can draw the common tangent depicted by the red line. Its inclination is the pressure $P = 0.118\text{MeV/fm}^3$ in the phase transition, which is shown by the horizontal red line in Fig. 1. The pressure is also determined from a crossing point on the black curve in Fig. 3, which shows the Gibbs energy per baryon as a function of pressure. The Gibbs energy on the crossing point is its equilibrated value in gaseous and liquid phases. To the contrary, the chemical potentials μ_N and μ_Λ are not equilibrated in the Maxwell construction of phase transition. As a matter of fact the black solid curves in Figs. 4 and 5, which show the chemical potentials as functions of pressure, expose discontinuities marked by the vertical red dotted lines, because the black dotted curves are the results in a region of the concave on Helmholtz energy and so are not realized physically. We have $\mu_N = 919.5$MeV and $\mu_\Lambda = 1099.9$MeV in gaseous phase but $\mu_N = 913.2$MeV and $\mu_\Lambda = 1106.4$MeV in liquid phase. Consequently, the Gibbs condition on the chemical potentials in phase equilibrium is not satisfied. The black curves in Fig. 6 show the baryon fractions ρ_{bB}/ρ_T as functions of the total baryon density. As the SHM becomes denser, the fraction of Λ decreases while the fraction of Ξ increases, although the total strangeness of SHM is constant. The fraction of Σ is too low to be apparent in the figure.

For the micro-canonical ensemble of a constant pressure P, a given total baryon density ρ_T and a definite strangeness fraction f_S, we have to solve the 7th-rank simultaneous nonlinear equations (4)-(7) and (13)-(15) so that the effective masses, the vector potentials and the chemical potentials of nucleon and lambda, and the internal temperature of

SHM are determined. The quantity characterizing the thermodynamic process under a constant pressure is the enthalpy H:

$$\tilde{H} = H/V = \mathcal{E} + P, \tag{16}$$

where the energy density is given by

$$\begin{aligned}\mathcal{E} &= \sum_{B=N,\Lambda,\Sigma,\Xi} \left\{ \gamma_B \int_0^\infty \frac{d^3\mathbf{k}}{(2\pi)^3} E^*_{kB} \left[n_{kB}\left(m^*_B, v_B; \mu_B, T\right) + \bar{n}_{kB}\left(m^*_B, v_B; \mu_B, T\right)\right] + V_B \rho_{bB} \right\} \\ &+ \frac{1}{2} m_\sigma^2 \langle\sigma\rangle^2 - \frac{1}{2} m_\omega^2 \langle\omega_0\rangle^2 + \frac{1}{2} m_{\sigma^*}^2 \langle\sigma^*\rangle^2 - \frac{1}{2} m_\phi^2 \langle\phi_0\rangle^2 . \end{aligned} \tag{17}$$

The entropy per volume $\tilde{S} = S/V$ is calculated in terms of the Gibbs-Duhem relation $T\tilde{S} = \tilde{H} - \tilde{G}$, where $\tilde{G} = G/V = \sum_B \mu_B \rho_{bB}$ is the Gibbs energy per volume.

The black curve in Fig. 7 shows the entropy per baryon $S/A = \tilde{S}/\rho_T$ as a function of the enthalpy per baryon $H/A = \tilde{H}/\rho_T$ for $P = 0.05\text{MeV/fm}^3$ and $f_S = 0.5$. A dip or a convex intruder is due to liquid-gas phase transition. Because the entropy should be concave, the convex intruder is not realized physically. Although the SHM is a binary system, we can draw the common tangent depicted by the red line. Because of $\partial S/\partial H = 1/T$ we can determine the boiling temperature $T = 7.92\text{MeV}$ of SHM liquid from the inclination of the common tangent. The temperature is also determined from a crossing point on the black curve in Fig. 8, which shows the Gibbs energy per baryon $G/A = \tilde{G}/\rho_T$ as a function of temperature. The latent heat involved in the Maxwell construction of phase transition is a difference between the two enthalpies on the red crosses in Fig. 7. The black curve in Fig. 9 shows the caloric curve, the internal temperature T of SHM as a function of the excitation energy per baryon E^*/A, which is obtained by subtracting the binding energy of cold ($T = 0$) SHM [18] from $\mathcal{E}/\rho_T$. The dotted part is the spurious result in a region of the convex intruder on entropy, and so is replaced by the horizontal red line of the boiling temperature. The black solid curves in Figs. 10-12 show the entropy per baryon and the chemical potentials μ_N and μ_Λ as functions of internal temperature of SHM. They expose the discontinuities at $T = 7.92\text{MeV}$ marked by the horizontal red dotted lines, because the black dotted curves are the spurious results in a region of the convex intruder in Fig. 7. We have $\mu_N = 922.2\text{MeV}$ and $\mu_\Lambda = 1102.1\text{MeV}$ in gaseous phase but $\mu_N = 915.1\text{MeV}$ and $\mu_\Lambda = 1109.3\text{MeV}$ in liquid phase. Consequently, we see again that the chemical potentials in the Maxwell construction of phase transition are not equilibrated.

3 Gibbs construction of phase transition

As seen in Figs. 4 and 5 the common tangent prescription is not appropriate to the binary nuclear system as SHM because the Gibbs condition on the two independent chemical potentials is not satisfied. So as to construct the physically reasonable liquid-gas phase transition in the canonical ensemble of SHM, we have to calculate the following 11th-rank simultaneous nonlinear equations. The four equations of them determine the vector potentials and the effective masses of nucleon and lambda in gaseous phase marked by suffix g:

$$\rho_{bN}^{(g)} + \sum_{Y=\Sigma,\Xi} \left(\frac{g_{YY\omega}^{(g)*}}{g_{NN\omega}^{(g)*}} - \frac{g_{YY\phi}^{(g)*}}{g_{\Lambda\Lambda\phi}^{(g)*}} \frac{g_{\Lambda\Lambda\omega}^{(g)*}}{g_{NN\omega}^{(g)*}} \right) \rho_{bY}^{(g)} - \left(\frac{m_\omega}{g_{NN\omega}^{(g)*}} \right)^2 V_N^{(g)} + \left(\frac{m_\phi}{g_{\Lambda\Lambda\phi}^{(g)*}} \right)^2 \frac{g_{\Lambda\Lambda\omega}^{(g)*}}{g_{NN\omega}^{(g)*}} C_{N\Lambda\,\omega}^{(g)} = 0, \tag{18}$$

$$\rho_{b\Lambda}^{(g)} + \sum_{Y=\Sigma,\Xi} \frac{g_{YY\phi}^{(g)*}}{g_{\Lambda\Lambda\phi}^{(g)*}} \rho_{bY}^{(g)} - \left(\frac{m_\phi}{g_{\Lambda\Lambda\phi}^{(g)*}} \right)^2 C_{N\Lambda\,\omega}^{(g)} = 0, \tag{19}$$

$$\begin{aligned} &\sum_{B=N,\Sigma,\Xi} \frac{\partial m_B^{(g)*}}{\partial m_N^{(g)*}} M_B \rho_{sB}^{(g)} + \sum_{Y=\Sigma,\Xi} \frac{\partial V_Y^{(g)}}{\partial m_N^{(g)*}} \rho_{bY}^{(g)} + m_\sigma^2 \langle\sigma\rangle_g \frac{\partial \langle\sigma\rangle_g}{\partial m_N^{(g)*}} + m_{\sigma^*}^2 \langle\sigma^*\rangle_g \frac{\partial \langle\sigma^*\rangle_g}{\partial m_N^{(g)*}} \\ &+ \left(\frac{m_\omega}{g_{NN\omega}^{(g)*}} \right)^2 \frac{1}{g_{NN\omega}^{(g)*}} \frac{\partial g_{NN\omega}^{(g)*}}{\partial m_N^{(g)*}} \left(V_N^{(g)} \right)^2 + \left(\frac{m_\phi}{g_{\Lambda\Lambda\phi}^{(g)*}} \right)^2 \frac{1}{g_{\Lambda\Lambda\phi}^{(g)*}} \frac{\partial g_{\Lambda\Lambda\phi}^{(g)*}}{\partial m_N^{(g)*}} \left(C_{N\Lambda\,\omega}^{(g)} \right)^2 \\ &+ \left(\frac{m_\phi}{g_{\Lambda\Lambda\phi}^{(g)*}} \right)^2 \frac{1}{g_{NN\omega}^{(g)*}} \left(\frac{\partial g_{\Lambda\Lambda\omega}^{(g)*}}{\partial m_N^{(g)*}} - \frac{g_{\Lambda\Lambda\omega}^{(g)*}}{g_{NN\omega}^{(g)*}} \frac{\partial g_{NN\omega}^{(g)*}}{\partial m_N^{(g)*}} \right) V_N^{(g)} C_{N\Lambda\,\omega}^{(g)} = 0, \end{aligned} \tag{20}$$

$$\begin{aligned} &\sum_{Y} \frac{\partial m_Y^{(g)*}}{\partial m_\Lambda^{(g)*}} M_Y \rho_{sY}^{(g)} + \sum_{Y=\Sigma,\Xi} \frac{\partial V_Y^{(g)}}{\partial m_\Lambda^{(g)*}} \rho_{bY}^{(g)} + m_{\sigma^*}^2 \langle\sigma^*\rangle_g \frac{\partial \langle\sigma^*\rangle_g}{\partial m_\Lambda^{(g)*}} \\ &+ \left(\frac{m_\phi}{g_{\Lambda\Lambda\phi}^{(g)*}} \right)^2 \frac{1}{g_{NN\omega}^{(g)*}} \frac{\partial g_{\Lambda\Lambda\omega}^{(g)*}}{\partial m_\Lambda^{(g)*}} V_N^{(g)} C_{N\Lambda\,\omega}^{(g)} + \left(\frac{m_\phi}{g_{\Lambda\Lambda\phi}^{(g)*}} \right)^2 \frac{1}{g_{\Lambda\Lambda\phi}^{(g)*}} \frac{\partial g_{\Lambda\Lambda\phi}^{(g)*}}{\partial m_\Lambda^{(g)*}} \left(C_{N\Lambda\,\omega}^{(g)} \right)^2 = 0. \end{aligned} \tag{21}$$

It is noted again [18] that the mean-fields are expressed in terms of the effective masses and the vector potentials.

Similarly, the equations for liquid phase (marked by suffix l) are

$$\rho_{bN}^{(l)} + \sum_{Y=\Sigma,\Xi} \left(\frac{g_{YY\omega}^{(l)*}}{g_{NN\omega}^{(l)*}} - \frac{g_{YY\phi}^{(l)*}}{g_{\Lambda\Lambda\phi}^{(l)*}} \frac{g_{\Lambda\Lambda\omega}^{(l)*}}{g_{NN\omega}^{(l)*}} \right) \rho_{bY}^{(l)} - \left(\frac{m_\omega}{g_{NN\omega}^{(l)*}} \right)^2 V_N^{(l)} + \left(\frac{m_\phi}{g_{\Lambda\Lambda\phi}^{(l)*}} \right)^2 \frac{g_{\Lambda\Lambda\omega}^{(l)*}}{g_{NN\omega}^{(l)*}} C_{N\Lambda\,\omega}^{(l)} = 0, \tag{22}$$

$$\rho_{b\Lambda}^{(l)} + \sum_{Y=\Sigma,\Xi} \frac{g_{YY\phi}^{(l)*}}{g_{\Lambda\Lambda\phi}^{(l)*}} \rho_{bY}^{(l)} - \left(\frac{m_\phi}{g_{\Lambda\Lambda\phi}^{(l)*}} \right)^2 C_{N\Lambda\,\omega}^{(l)} = 0, \tag{23}$$

$$\sum_{B=N,\Sigma,\Xi} \frac{\partial m_B^{(l)*}}{\partial m_N^{(l)*}} M_B \rho_{sB}^{(l)} + \sum_{Y=\Sigma,\Xi} \frac{\partial V_Y^{(l)}}{\partial m_N^{(l)*}} \rho_{bY}^{(l)} + m_\sigma^2 \langle\sigma\rangle_l \frac{\partial \langle\sigma\rangle_l}{\partial m_N^{(l)*}} + m_{\sigma^*}^2 \langle\sigma^*\rangle_l \frac{\partial \langle\sigma^*\rangle_l}{\partial m_N^{(l)*}}$$
$$+ \left(\frac{m_\omega}{g_{NN\omega}^{(l)*}}\right)^2 \frac{1}{g_{NN\omega}^{(l)*}} \frac{\partial g_{NN\omega}^{(l)*}}{\partial m_N^{(l)*}} \left(V_N^{(l)}\right)^2 + \left(\frac{m_\phi}{g_{\Lambda\Lambda\phi}^{(l)*}}\right)^2 \frac{1}{g_{\Lambda\Lambda\phi}^{(l)*}} \frac{\partial g_{\Lambda\Lambda\phi}^{(l)*}}{\partial m_N^{(l)*}} \left(C_{N\Lambda\,\omega}^{(l)}\right)^2$$
$$+ \left(\frac{m_\phi}{g_{\Lambda\Lambda\phi}^{(l)*}}\right)^2 \frac{1}{g_{NN\omega}^{(l)*}} \left(\frac{\partial g_{\Lambda\Lambda\omega}^{(l)*}}{\partial m_N^{(l)*}} - \frac{g_{\Lambda\Lambda\omega}^{(l)*}}{g_{NN\omega}^{(l)*}} \frac{\partial g_{NN\omega}^{(l)*}}{\partial m_N^{(l)*}}\right) V_N^{(l)} C_{N\Lambda\,\omega}^{(l)} = 0, \tag{24}$$

$$\sum_Y \frac{\partial m_Y^{(l)*}}{\partial m_\Lambda^{(l)*}} M_Y \rho_{sY}^{(l)} + \sum_{Y=\Sigma,\Xi} \frac{\partial V_Y^{(l)}}{\partial m_\Lambda^{(l)*}} \rho_{bY}^{(l)} + m_{\sigma^*}^2 \langle\sigma^*\rangle_l \frac{\partial \langle\sigma^*\rangle_l}{\partial m_\Lambda^{(l)*}}$$
$$+ \left(\frac{m_\phi}{g_{\Lambda\Lambda\phi}^{(l)*}}\right)^2 \frac{1}{g_{NN\omega}^{(l)*}} \frac{\partial g_{\Lambda\Lambda\omega}^{(l)*}}{\partial m_\Lambda^{(l)*}} V_N^{(l)} C_{N\Lambda\omega}^{(l)} + \left(\frac{m_\phi}{g_{\Lambda\Lambda\phi}^{(l)*}}\right)^2 \frac{1}{g_{\Lambda\Lambda\phi}^{(l)*}} \frac{\partial g_{\Lambda\Lambda\phi}^{(l)*}}{\partial m_\Lambda^{(l)*}} \left(C_{N\Lambda\,\omega}^{(l)}\right)^2 = 0. \tag{25}$$

The other two equations determine the mixture of gas and liquid in the phase transition:

$$\rho_T = f_g\, \rho_T^{(g)} + (1 - f_g)\, \rho_T^{(l)}, \tag{26}$$

$$f_S \rho_T = f_g\, f_S^{(g)} \rho_T^{(g)} + (1 - f_g)\, f_S^{(l)} \rho_T^{(l)}, \tag{27}$$

where f_g $(0 \le f_g \le 1)$ is the ratio of gas. The baryon density and the strangeness fraction in gaseous and liquid phases are determined from Eqs. (13) and (14) using the following densities of each baryon:

$$\rho_{bB}^{(g)} = \gamma_B \int_0^\infty \frac{d^3\mathbf{k}}{(2\pi)^3} \left[n_{kB}\left(m_B^{(g)*}, v_B^{(g)}; \mu_B, T\right) - \bar{n}_{kB}\left(m_B^{(g)*}, v_B^{(g)}; \mu_B, T\right)\right], \tag{28}$$

$$\rho_{bB}^{(l)} = \gamma_B \int_0^\infty \frac{d^3\mathbf{k}}{(2\pi)^3} \left[n_{kB}\left(m_B^{(l)*}, v_B^{(l)}; \mu_B, T\right) - \bar{n}_{kB}\left(m_B^{(l)*}, v_B^{(l)}; \mu_B, T\right)\right]. \tag{29}$$

The last equation imposes an equilibrium condition on pressures in gaseous and liquid phases:

$$\frac{1}{6\pi^2} \sum_{B=N,\Lambda,\Sigma,\Xi} \gamma_B \int_0^\infty dk\, \frac{k^4}{E_{kB}^*} \left[n_{kB}\left(m_B^{(g)*}, v_B^{(g)}; \mu_B, T\right) + \bar{n}_{kB}\left(m_B^{(g)*}, v_B^{(g)}; \mu_B, T\right)\right]$$
$$- \frac{1}{2} m_{\sigma^*}^2 \langle\sigma\rangle_g^2 + \frac{1}{2} m_\omega^2 \langle\omega_0\rangle_g^2 - \frac{1}{2} m_\sigma^2 \langle\sigma^*\rangle_g^2 + \frac{1}{2} m_\phi^2 \langle\phi_0\rangle_g^2$$
$$= \frac{1}{6\pi^2} \sum_{B=N,\Lambda,\Sigma,\Xi} \gamma_B \int_0^\infty dk\, \frac{k^4}{E_{kB}^*} \left[n_{kB}\left(m_B^{(l)*}, v_B^{(l)}; \mu_B, T\right) + \bar{n}_{kB}\left(m_B^{(l)*}, v_B^{(l)}; \mu_B, T\right)\right]$$
$$- \frac{1}{2} m_\sigma^2 \langle\sigma\rangle_l^2 + \frac{1}{2} m_\omega^2 \langle\omega_0\rangle_l^2 - \frac{1}{2} m_{\sigma^*}^2 \langle\sigma^*\rangle_l^2 + \frac{1}{2} m_\phi^2 \langle\phi_0\rangle_l^2\,. \tag{30}$$

Solving Eqs. (18)-(27) and (30) simultaneously, we have the effective masses and the vector potentials of nucleon and lambda in each of phases, the chemical potentials of nucleon and lambda, and the ratio of gas (or liquid) in the phase transition. For numerical calculations we have used the globally convergent Newton algorism in Ref. [24]. The trial values for solutions are easily found from the corresponding results in the common tangent method.

The numerical results for $f_S = 0.5$ and $T = 10$MeV are shown by the blue curves in Figs. 1-6. We can see that the Gibbs condition on pressure and chemical potentials recovers the convex minimized Helmholtz energy lying below the common tangent, because the Gibbs condition in isothermal process is derived by minimizing the Helmholtz energy through the fundamental thermodynamic equation $dF = -SdT - PdV + \sum_B \mu_B dN_B$. Consequently, the pressure in Fig. 1, which is the value of the right or left hand side of Eq. (30), increases slowly in the phase transition from gas to liquid against the constant pressure from the common tangent. Moreover, the region of phase transition between $\rho_T = 0.0095\text{fm}^{-3}$ and 0.181fm^{-3} is wider than the one between $\rho_T = 0.016\text{fm}^{-3}$ and 0.174fm^{-3} from the common tangent. The Gibbs energy in Fig. 3 is also minimized as a function pressure because of $G/A = F/A + P/\rho_T$. The chemical potentials in Figs. 4 and 5 become the continuous functions of pressure, because their values move from the black solid curves to the blue curves and vise versa at the blue dots as the pressure increases. These are natural results from the proper calculus of phase transition. We can see in Fig. 6 that the Gibbs condition on phase equilibrium also affects baryon fractions in phase transition. The N and Ξ become richer while Λ becomes poorer. The result is due to our choice [23] of hyperon-hyperon interaction. Because we assume a weak $\Lambda\Lambda$ attraction, poorer Λ or richer Ξ is favorable to the minimized Helmholtz energy. Figure 13 shows the ratio of liquid $f_l = 1 - f_g$ and the strangeness fractions of gaseous and liquid phases $f_S^{(g)}$ and $f_S^{(l)}$ in Eq. (27). Both the strangeness fractions become higher in the phase transition from gas to liquid, although the gaseous phase has much higher strangeness than the liquid phase.

Here we have to discuss the order of the phase transition. Because the black curve and the blue dashed curve in Fig. 3 connect smoothly on the two blue dots, $\partial G/\partial P$ has no discontinuity. Reference [7] therefore certifies that the liquid-gas phase transition in a binary nuclear system is the second order. However, the argument is not consistent with the Gibbs condition, to which each of the chemical potentials rather than the Gibbs energy is relevant. We see in Figs. 4 and 5 that $\partial\mu_N/\partial P$ and $\partial\mu_\Lambda/\partial P$ have discontinuities on the blue dots or the transition points. It is therefore concluded against Ref. [7] that the phase transition is the first order.

Next, we investigate the dependence of liquid-gas phase transition on the strangeness fraction. Figure 14 shows the pressure-density isotherms of $T = 10$MeV for several values of f_S. The physically realized pressures in the phase transitions are the solid curves from Eq. (30), while the dashed curves are the spurious results from Eq. (15). Although

the dashed curve of $f_S = 1.2$ does not behave as van der Waals equation of state, the minimization of the Helmholtz energy still leads to the liquid-gas phase transition. Figure 15 shows the section of binodal surface at $T = 10$MeV. Between $f_S = 1.45$ and $f_S = 1.505$ there are upper limits on the baryon density, above which we find no solutions of the simultaneous equations (18)-(27) and (30). Consequently, there is no critical point, on which the liquid branch connects with the gas branch. The absence of critical point was found first in Ref. [8] and was recovered in the recent works [1,11] for asymmetric nuclear matter. It was due to the density-dependent [8] or the momentum-dependent [11] effective NN interaction. The field-dependent effective meson-nucleon coupling constants in Ref. [1] are also derived from the momentum-dependent coupling constants [25] and lead to effective density dependencies. The absence of critical point in SHM was found first in Ref. [22] and has been recovered in the present work that uses the field-dependent effective meson-nucleon coupling constants too. The gas branch in the binodal surface shows a backbend with a bending point at $f_S = 1.636$, above which there is no SHM liquid. Consequently, between $f_S = 1.505$ and $f_S = 1.636$ we can see the retrograde condensation. For an example Fig. 16 shows the ratio of liquid as a function of pressure for strangeness fraction $f_S = 1.57$.

Next, we construct the physically reasonable liquid-gas phase transition in the micro-canonical ensemble of SHM. For the purpose we have to solve Eqs. (18)-(27) under the Gibbs condition on pressures in the equilibrated gaseous and liquid phases:

$$\begin{aligned} P &= \frac{1}{6\pi^2} \sum_{B=N,\Lambda,\Sigma,\Xi} \gamma_B \int_0^\infty dk \, \frac{k^4}{E^*_{kB}} \left[n_{kB} \left(m_B^{(g)*}, v_B^{(g)}; \mu_B, T \right) + \bar{n}_{kB} \left(m_B^{(g)*}, v_B^{(g)}; \mu_B, T \right) \right] \\ &\quad - \frac{1}{2} m_\sigma^2 \langle \sigma \rangle_g^2 + \frac{1}{2} m_\omega^2 \langle \omega_0 \rangle_g^2 - \frac{1}{2} m_{\sigma^*}^2 \langle \sigma^* \rangle_g^2 + \frac{1}{2} m_\phi^2 \langle \phi_0 \rangle_g^2 . \end{aligned} \tag{31}$$

$$\begin{aligned} P &= \frac{1}{6\pi^2} \sum_{B=N,\Lambda,\Sigma,\Xi} \gamma_B \int_0^\infty dk \, \frac{k^4}{E^*_{kB}} \left[n_{kB} \left(m_B^{(l)*}, v_B^{(l)}; \mu_B, T \right) + \bar{n}_{kB} \left(m_B^{(l)*}, v_B^{(l)}; \mu_B, T \right) \right] \\ &\quad - \frac{1}{2} m_\sigma^2 \langle \sigma \rangle_l^2 + \frac{1}{2} m_\omega^2 \langle \omega_0 \rangle_l^2 - \frac{1}{2} m_{\sigma^*}^2 \langle \sigma^* \rangle_l^2 + \frac{1}{2} m_\phi^2 \langle \phi_0 \rangle_l^2 . \end{aligned} \tag{32}$$

Solving these 12th-rank simultaneous nonlinear equations for a constant pressure P, we have the effective masses and the vector potentials of nucleon and lambda in each of phases, the chemical potentials of nucleon and lambda, the ratio of gaseous (or liquid) phase, and the internal temperature of SHM. The trial values for solutions are easily found from the corresponding results in the common tangent prescription. Using the results, the total energy density is given by

$$\mathcal{E} = f_g \, \mathcal{E}_g + (1 - f_g) \, \mathcal{E}_l, \tag{33}$$

where the energy densities of gaseous and liquid phases in the phase transition are

$$\begin{aligned}\mathcal{E}_g &= \sum_{B=N,\Lambda,\Sigma,\Xi}\gamma_B\int_0^\infty\frac{d^3\mathbf{k}}{(2\pi)^3}E_{kB}^{(g)*}\left[n_{kB}\left(m_B^{(g)*},v_B^{(g)};\mu_B,T\right)+\bar{n}_{kB}\left(m_B^{(g)*},v_B^{(g)};\mu_B,T\right)\right]\\ &+\sum_{B=N,\Lambda,\Sigma,\Xi}V_B^{(g)}\rho_{bB}^{(g)}+\frac{1}{2}m_\sigma^2\langle\sigma\rangle_g^2-\frac{1}{2}m_\omega^2\langle\omega_0\rangle_g^2+\frac{1}{2}m_{\sigma^*}^2\langle\sigma^*\rangle_g^2-\frac{1}{2}m_\phi^2\langle\phi_0\rangle_g^2\,, \quad (34)\end{aligned}$$

$$\begin{aligned}\mathcal{E}_l &= \sum_{B=N,\Lambda,\Sigma,\Xi}\gamma_B\int_0^\infty\frac{d^3\mathbf{k}}{(2\pi)^3}E_{kB}^{(l)*}\left[n_{kB}\left(m_B^{(l)*},v_B^{(l)};\mu_B,T\right)+\bar{n}_{kB}\left(m_B^{(l)*},v_B^{(l)};\mu_B,T\right)\right]\\ &+\sum_{B=N,\Lambda,\Sigma,\Xi}V_B^{(l)}\rho_{bB}^{(l)}+\frac{1}{2}m_\sigma^2\langle\sigma\rangle_l^2-\frac{1}{2}m_\omega^2\langle\omega_0\rangle_l^2+\frac{1}{2}m_{\sigma^*}^2\langle\sigma^*\rangle_l^2-\frac{1}{2}m_\phi^2\langle\phi_0\rangle_l^2\,. \quad (35)\end{aligned}$$

The numerical results for $f_S = 0.5$ and $P = 0.05\text{MeV/fm}^3$ are shown by the blue curves in Figs. 7-12. We can see in Fig. 7 that the Gibbs condition on temperature and chemical potentials recovers the maximized entropy lying above the common tangent, because the Gibbs condition in micro-canonical ensemble is derived from the maximization of entropy. Because the entropy is concave, the region of phase transition between $H/A = 1019.7\text{MeV}$ and 1049.1MeV marked by the two blue dots is wider than the one from the common tangent between $H/A = 1022\text{MeV}$ and 1046MeV marked by the two red crosses. The concavity also produces the graduate increase of caloric curve in the phase transition against the constant boiling temperature from the common tangent. We see in Fig. 8 that the Gibbs condition leads to the minimum Gibbs energy in the phase transition. The entropy and the chemical potentials in Figs. 10-12 become the continuous functions of temperature, because their values move from the black solid curves to the blue curves and vise versa at the blue dots as the temperature increases. These are natural results from the proper calculus of phase transition. On the other hand, their derivatives have discontinuities on the blue dots or the transition points. Although Ref. [22] certifies that the phase transition is the second order because of the discontinuity in $\partial S/\partial T$ or the specific heat capacity, we certify that the phase transition is the first order because of the discontinuities in $\partial\mu_N/\partial T$ and $\partial\mu_\Lambda/\partial T$. Moreover, we have a finite latent heat, which is a difference between the two enthalpies on the blue dots in Fig. 7. Figure 17 shows the boiling temperature of SHM liquid (the blue curve) and the condensed temperature of SHM gas (the red curve) as functions of the strangeness fraction. The nuclear liquid of strangeness $f_S^{(l)} = 0.5$ begins to evaporate at $T = 6.0\text{MeV}$ into highly strange nuclear gas of $f_S^{(g)} = 1.34$. When the evaporation completes at $T = 8.92\text{MeV}$, the liquid phase has a rather low strangeness $f_S^{(l)} = 0.1385$.

4 Summary

We have developed new calculus of the liquid-gas phase transition in the canonical and micro-canonical ensembles of SHM based on the RMF model in Refs. [18] and [23]. It is different from the geometrical construction used widely in literature. For canonical ensemble the pressure and the chemical potentials are determined from definite values of temperature, strangeness and baryon density. The pressure increases in the phase transition from gas to liquid against the constant value from the Maxwell construction of phase equilibrium. The Helmholtz energy is minimized and so lies below the common tangent. Due to the convexity of Helmholtz energy, the region of phase transition is wider than that from the Maxwell construction. The liquid and gas branches in the section of binodal surface are connected on the normal state $f_S = 0$, but there is no critical point. Because the gas branch shows a backbend, the retrograde condensation in SHM has been proved. For micro-canonical ensemble of SHM, the temperature and the chemical potentials are determined from definite values of pressure, strangeness and baryon density. The resultant entropy is maximized and so lies above the common tangent, while the Gibbs energy is minimized. Due to the concavity of entropy, the boiling temperature of nuclear liquid increases slowly against the constant value from the Maxwell construction. We also investigate the change of strangeness in gaseous and liquid phases during the boiling process. Because at transition points there are discontinuities in the derivatives of chemical potentials $\partial\mu_N/\partial P$ and $\partial\mu_\Lambda/\partial P$ in canonical ensemble and $\partial\mu_N/\partial T$ and $\partial\mu_\Lambda/\partial T$ in micro-canonical ensemble, we conclude against the preceding works that the phase transition is the first order.

References

[1] K. Miyazaki, Mathematical Physics Preprint Archive (mp_arc) 07-92.

[2] K. Miyazaki, Mathematical Physics Preprint Archive (mp_arc) 07-141.

[3] J. Richert and P. Wagner, Phys. Rep. **350** (2001) 1 [arXiv:nucl-th/0009023].

[4] S.D. Gupta, A.Z. Mekjian and M.B. Tsang, *Advances in Nuclear Physics*, Vol. **26** (Kluwer Academic, 2001) [arXiv:nucl-th/0009033].

[5] V.E. Viola *et al.*, Phys. Rep. **434** (2006) 1 [arXiv:nucl-ex/0604012].

[6] V.A. Karnaukhov, Phys. Elem. Part. Atom. Nucl. **37** (2006) 312 [http://www1.jinr.ru/Pepan/Pepan_index.html].

[7] H. Műller and B.D. Serot, Phys. Rev. C **52** (1995) 2072 [arXiv:nucl-th/9505013].

[8] W.L. Qian, R-K. Su and P. Wang, Phys. Lett. B **491** (2000) 90 [arXiv:nucl-th/0008057].

[9] P.K. Panda, G. Klein, D.P. Menezes and C. Providência, Phys. Rev. C **68** (2003) 015201 [arXiv:nucl-th/0306045].

[10] P. Wang, D.B. Leinweber, A.W. Thomas and A.G. Williams, Nucl. Phys. A **748** (2005) 226 [arXiv:nucl-th/0407057].

[11] J. Xu. L-W. Chen, B-A. Li and H-R. Ma, arXiv:nucl-th/0702085.

[12] J. Schaffner, C.B. Dover, A. Gal, C. Greiner and H. Stőker, Phys. Rev. Lett. **71** (1993) 1328.

[13] V.G.J. Stoks and T.-S.H. Lee, Phys. Rev. C **60** (1999) 024006, [arXiv:nucl-th/9901030].

[14] P. Wang, R.K. Su, H.Q. Song and L.L. Zhang, Nucl. Phys. A **653** (1999) 166.

[15] J. Schaffner-Bielich and A. Gal, Phys. Rev. C **62** (2000) 034311, [arXiv:nucl-th/0005060].

[16] P. Wang, Z.Y. Zhang, Y.W. Yu, R.K. Su, H.Q. Song, Nucl. Phys. A **688** (2001) 791.

[17] I. Zakout, H.R. Jaqaman, H. Stőker and W. Greiner, J. Phys. G **27** (2001) 1939, [arXiv:nucl-th/005005].

[18] K. Miyazaki, Mathematical Physics Preprint Archive (mp_arc) 05-216.

[19] L. Yang, W.L. Qian, R.K. Su and H.Q. Song, Phys. Rev. C **70** (2004) 045207 [arXiv:nucl-th/0311017];

[20] P. Wang. D.B. Leinweber, A.W. Thomas and A.G. Williams, Nucl. Phys. A **744** (2004) 273 [arXiv:nucl-th/0404079].

[21] P. Wang. D.B. Leinweber, A.W. Thomas and A.G. Williams, Phys. Rev. C **70** (2004) 055204 [arXiv:nucl-th/0407056].

[22] L. Yang, S.Y. Yin, W.L. Qian, and R.K. Su, Phys. Rev. C **73** (2006) 025203 [arXiv:nucl-th/0506060];

[23] K. Miyazaki, Mathematical Physics Preprint Archive (mp_arc) 06-175.

[24] W.H. Press, S.A. Teukolsky, W.T. Vetterling and B.P. Flannery, Numerical Recipes in C 2nd edition, 1992, Cambridge University Press [http://www.nr.com/].

[25] K. Miyazaki, Mathematical Physics Preprint Archive (mp_arc) 06-175.

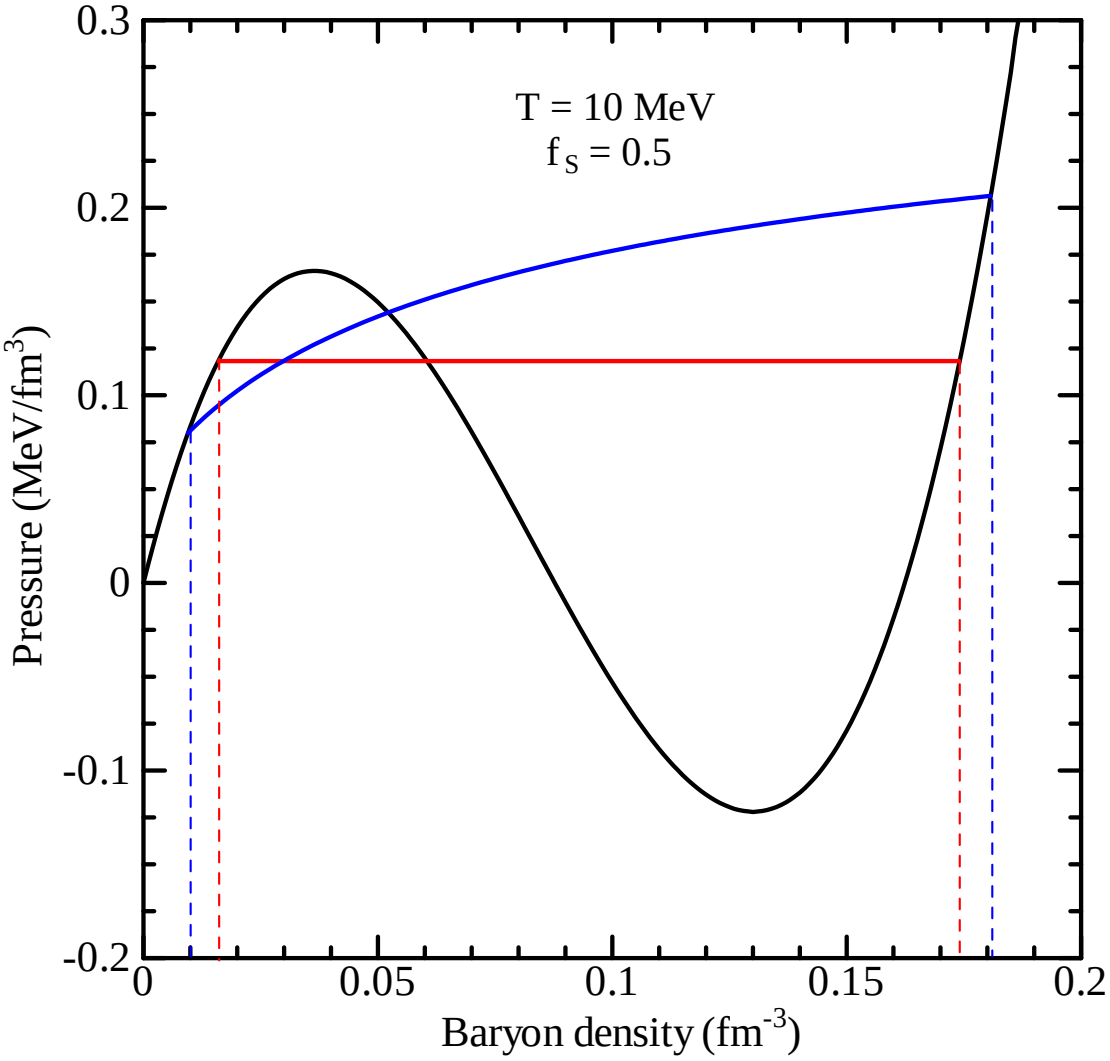

Figure 1: The pressure-density isotherm of temperature $T = 10$MeV for strangeness fraction $f_S = 0.5$. The black curve is the result from Eq. (15). The horizontal red line is the pressure in the phase transition derived from the common tangent prescription in Fig. 2. The blue curve is the pressure in the phase transition from Eq. (30). The vertical red and blue dashed lines indicate the regions of phase transition.

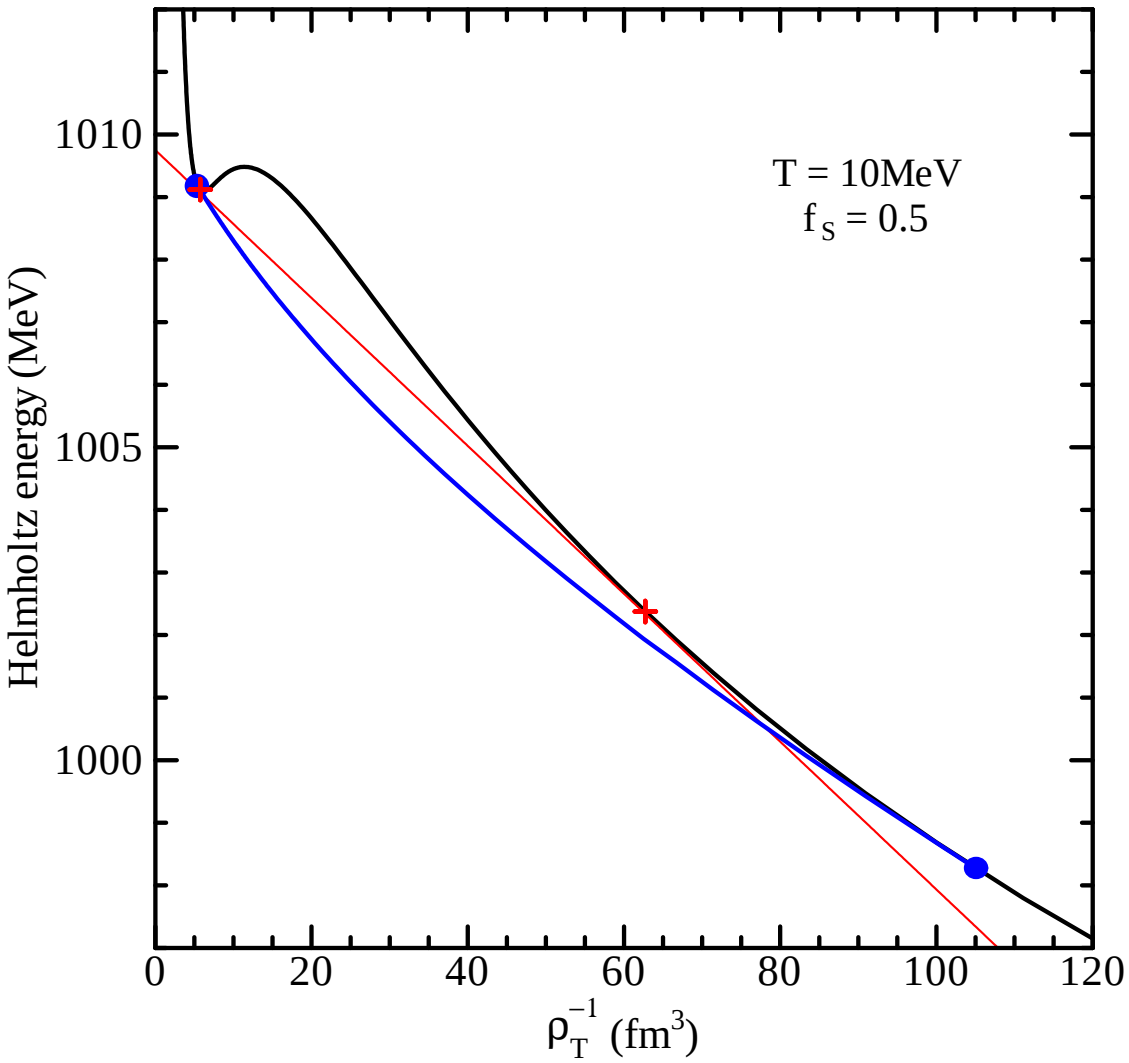

Figure 2: The Helmholtz energy per baryon as a function of volume for strangeness fraction $f_S = 0.5$ and temperature $T = 10$MeV. The black curve is the result corresponding to the black curve in Fig. 1. The red line is the common tangent that contacts with the black curve on the two red crosses. The blue curve between the two blue dots is the minimized Helmholtz energy in liquid-gas phase transition, which satisfies the Gibbs condition on phase equilibrium.

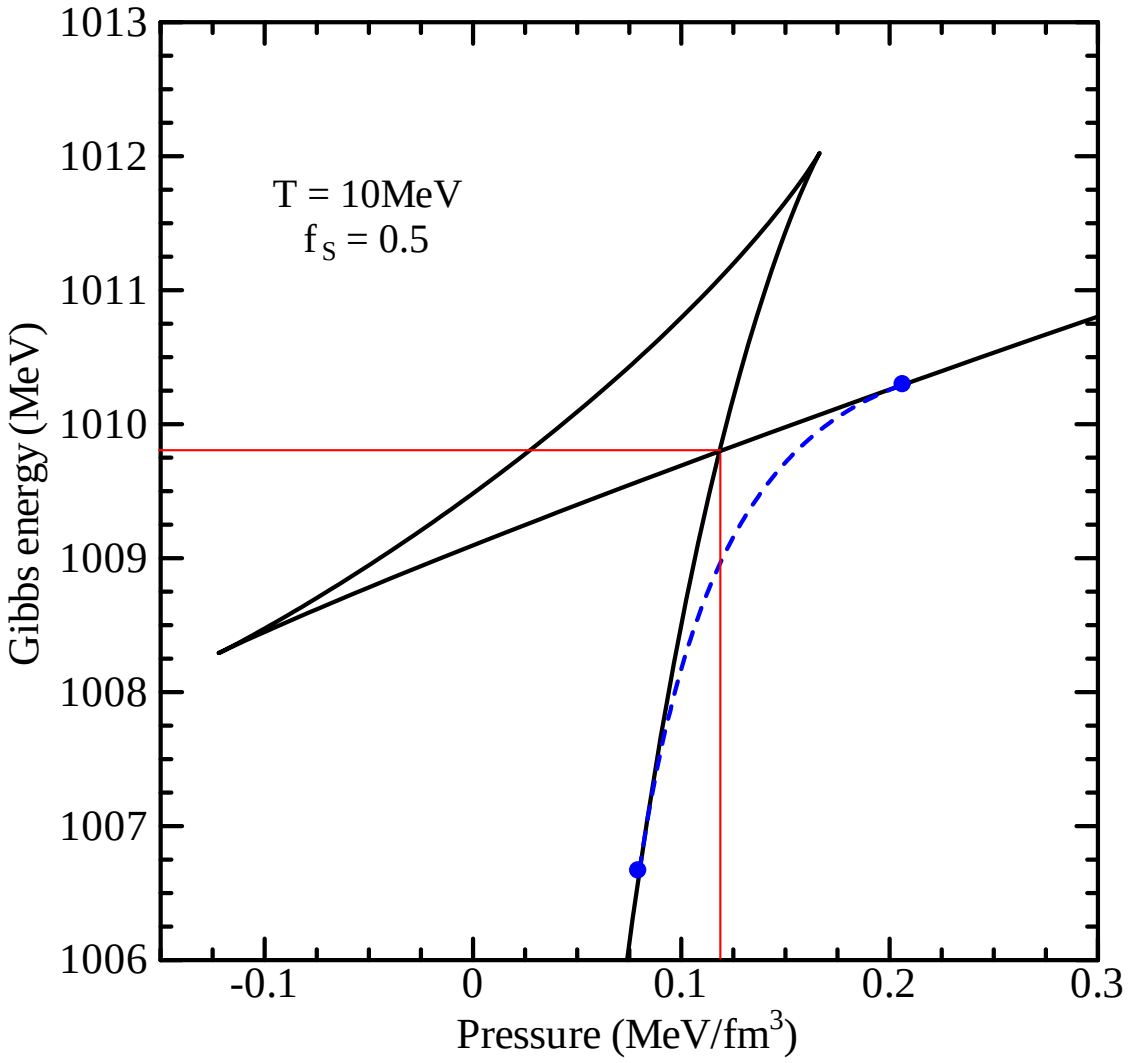

Figure 3: The Gibbs energy per baryon as a function of pressure for strangeness fraction $f_S = 0.5$ and temperature $T = 10$MeV. The black curve is the result corresponding to the black curve in Fig. 2. It has a crossing point denoted by the red line. The blue dashed curve between the two blue dots is the Gibbs energy in liquid-gas phase transition, which satisfies the Gibbs condition on phase equilibrium.

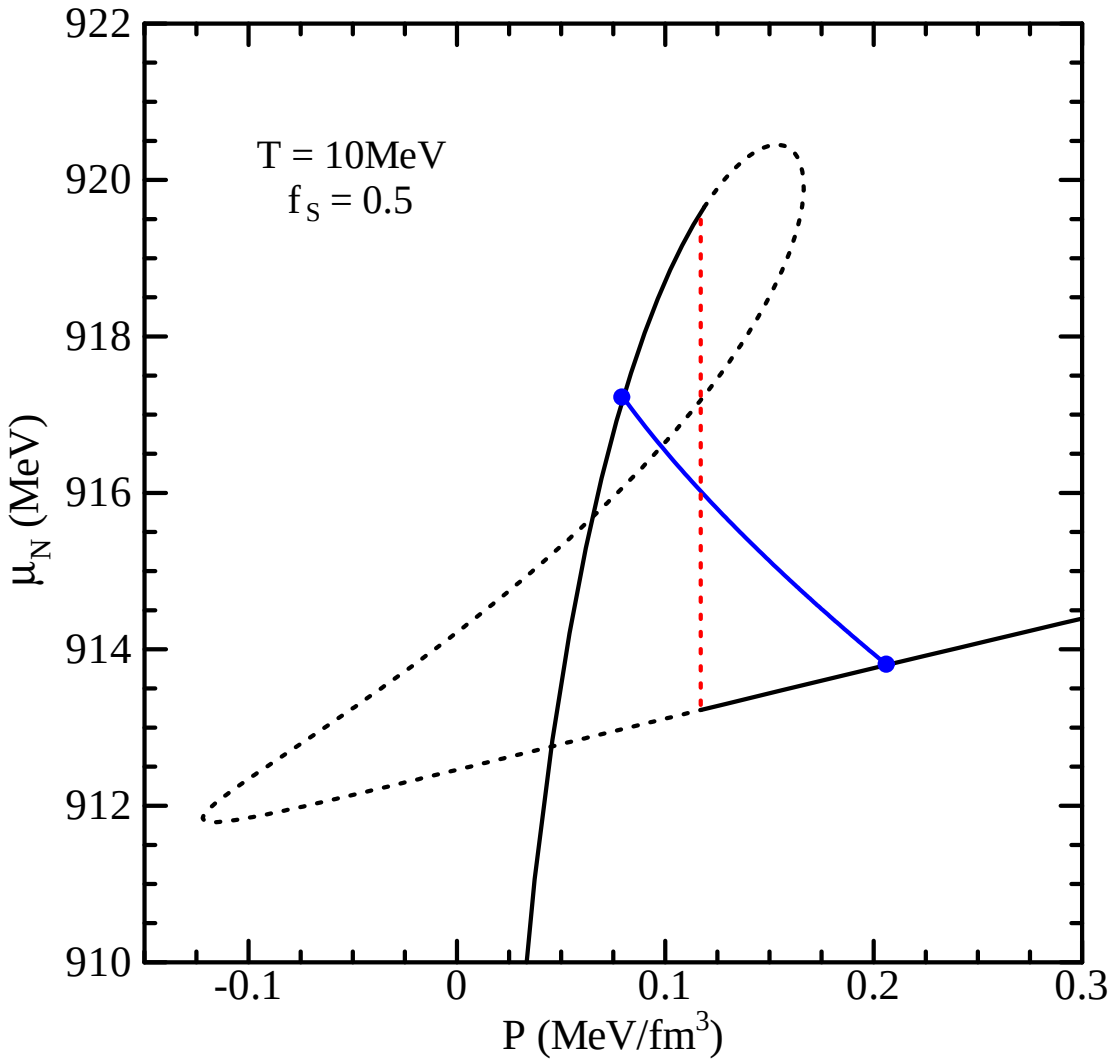

Figure 4: The nucleon chemical potential as a function of pressure for strangeness fraction $f_S = 0.5$ and temperature $T = 10$MeV. The black dotted curve is the result in a region of the concave on Helmholtz energy in Fig. 2 and so is not realized. Consequently, the black solid curve exposes a discontinuity marked by the vertical red dotted line. The blue curve is the chemical potential in liquid-gas phase transition, which satisfies the Gibbs condition on phase equilibrium.

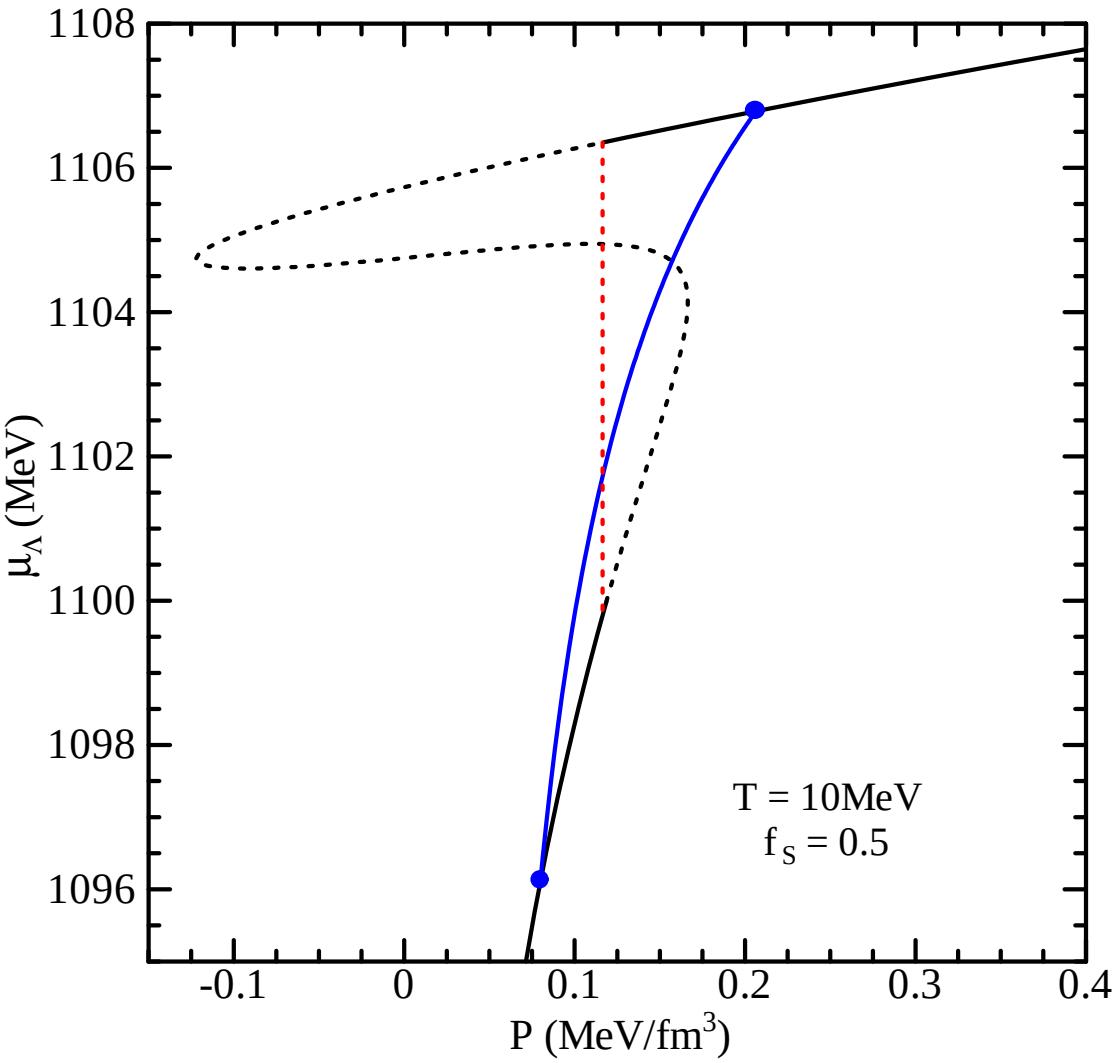

Figure 5: The same as Fig. 4 but for μ_Λ.

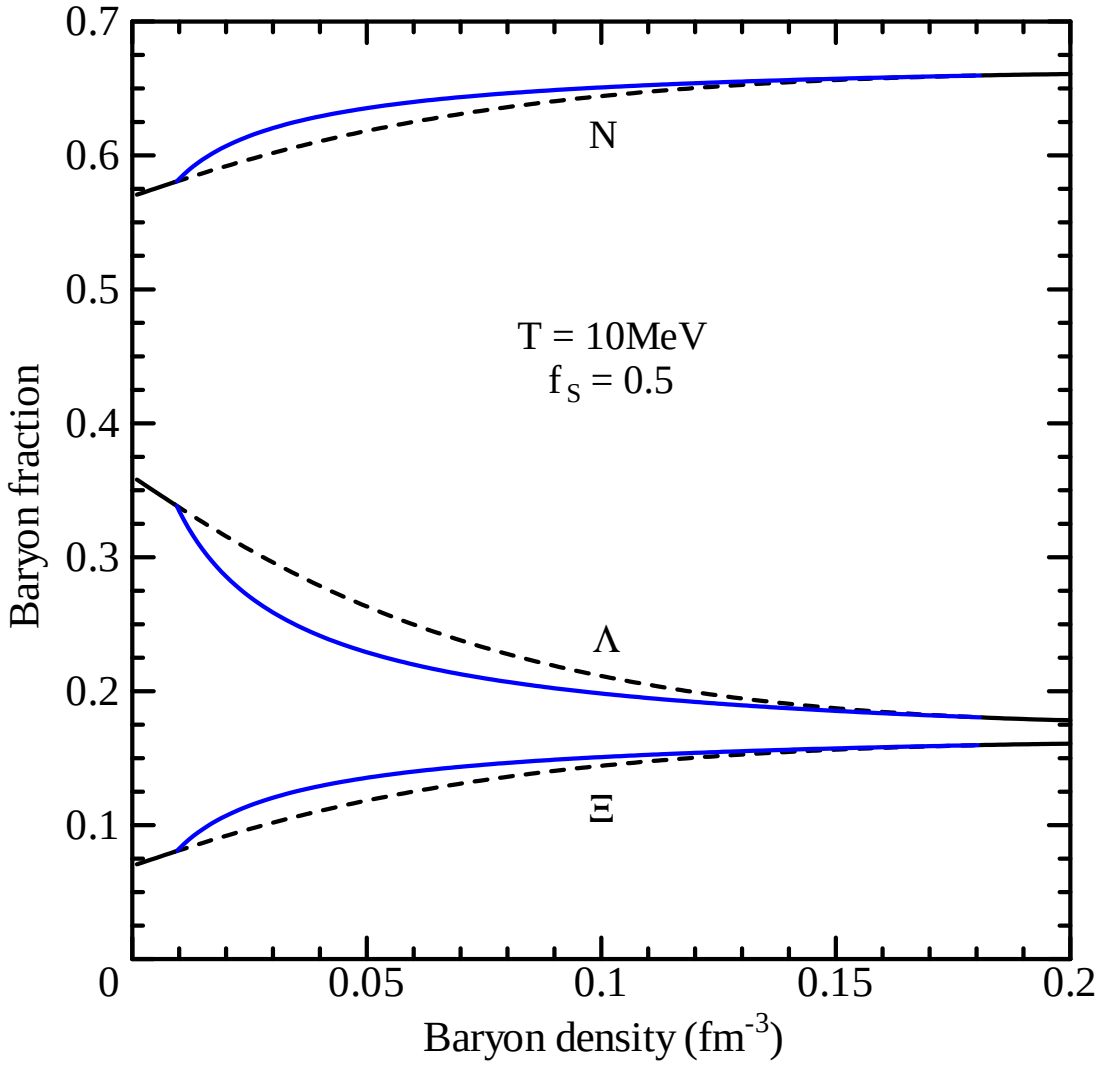

Figure 6: The baryon fractions ρ_{bB}/ρ_T as functions of the total baryon density. The black curves are the results corresponding to the black curve in Fig. 2. The blue curves are the fractions in liquid-gas phase transition, which satisfies the Gibbs condition on phase equilibrium. The fraction of Σ is too small to be apparent in the figure.

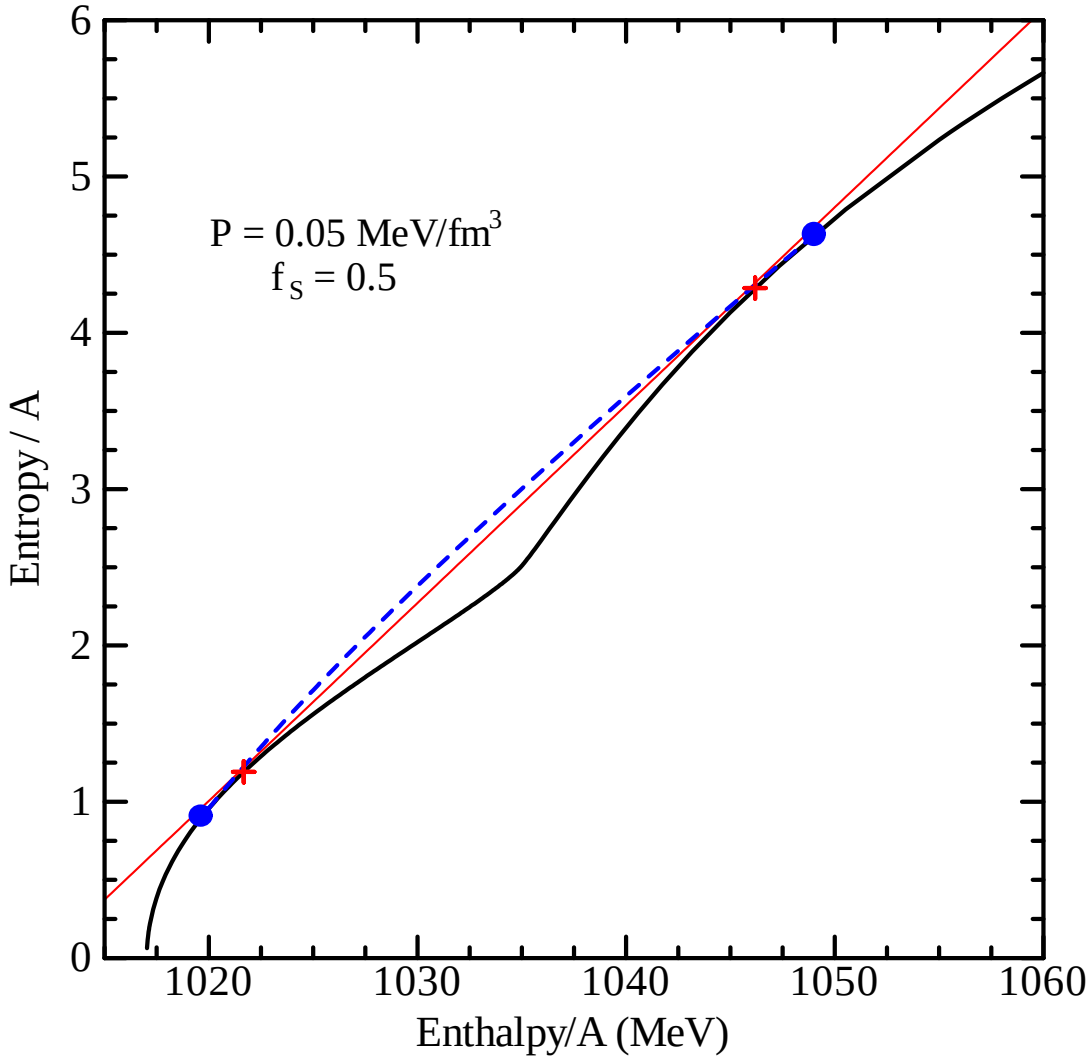

Figure 7: The black curve is the entropy per baryon as a function of the enthalpy per baryon for SHM of strangeness fraction $f_S = 0.5$ and pressure $P = 0.05\text{MeV/fm}^3$. The red line is the common tangent that contacts with the black curve on the two red crosses. The blue dashed curve between the two blue dots is the maximized entropy in liquid-gas phase transition, which satisfies the Gibbs condition on phase equilibrium.

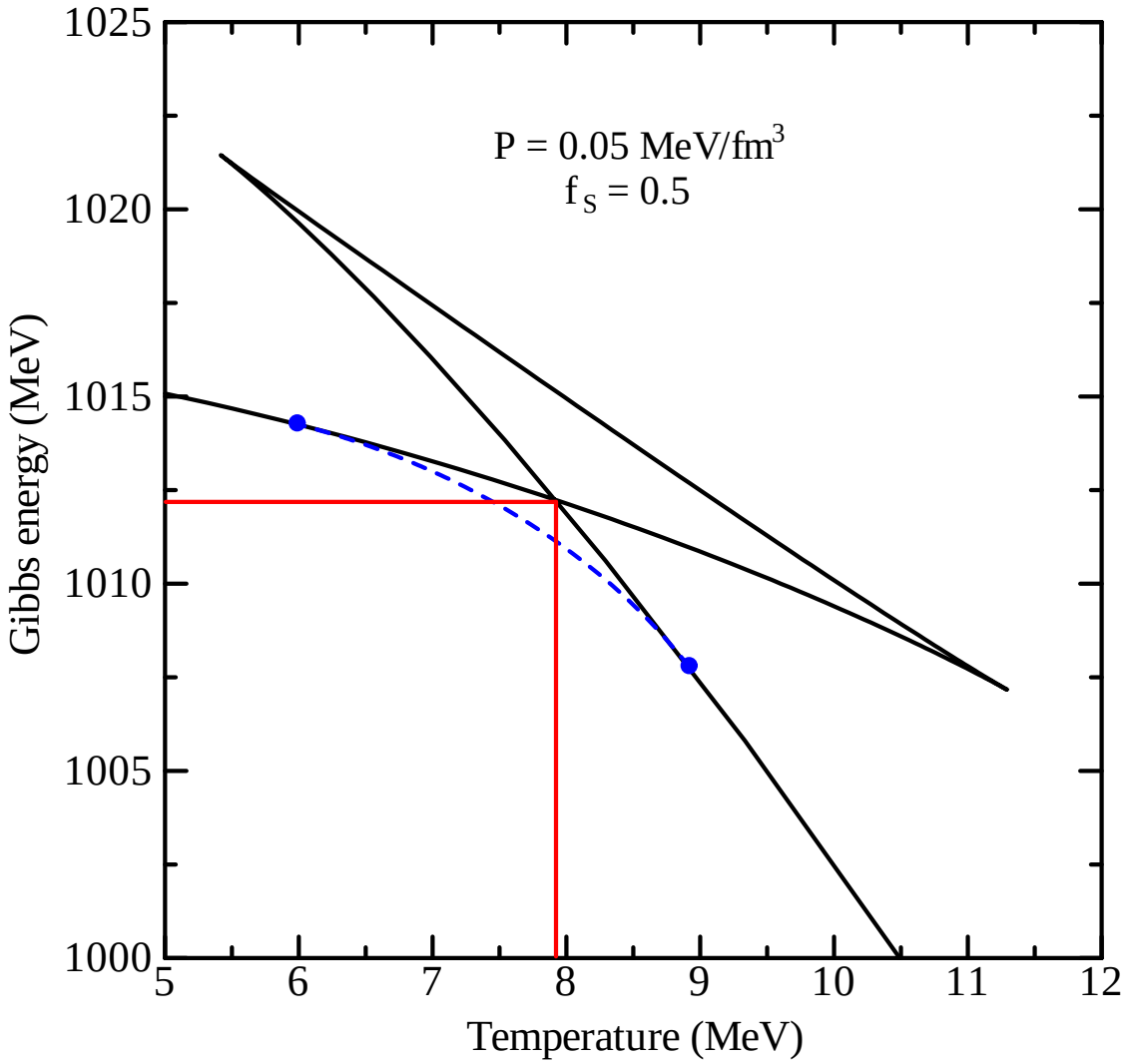

Figure 8: The Gibbs energy per baryon as a function of temperature for $f_S = 0.5$ and $P = 0.05\text{MeV/fm}^3$. The black curve is the result derived from the black curve in Fig. 7. It has a crossing point marked by the red line. The blue dashed curve between the two blue dots is the Gibbs energy in liquid-gas phase transition, which satisfies the Gibbs condition on phase equilibrium.

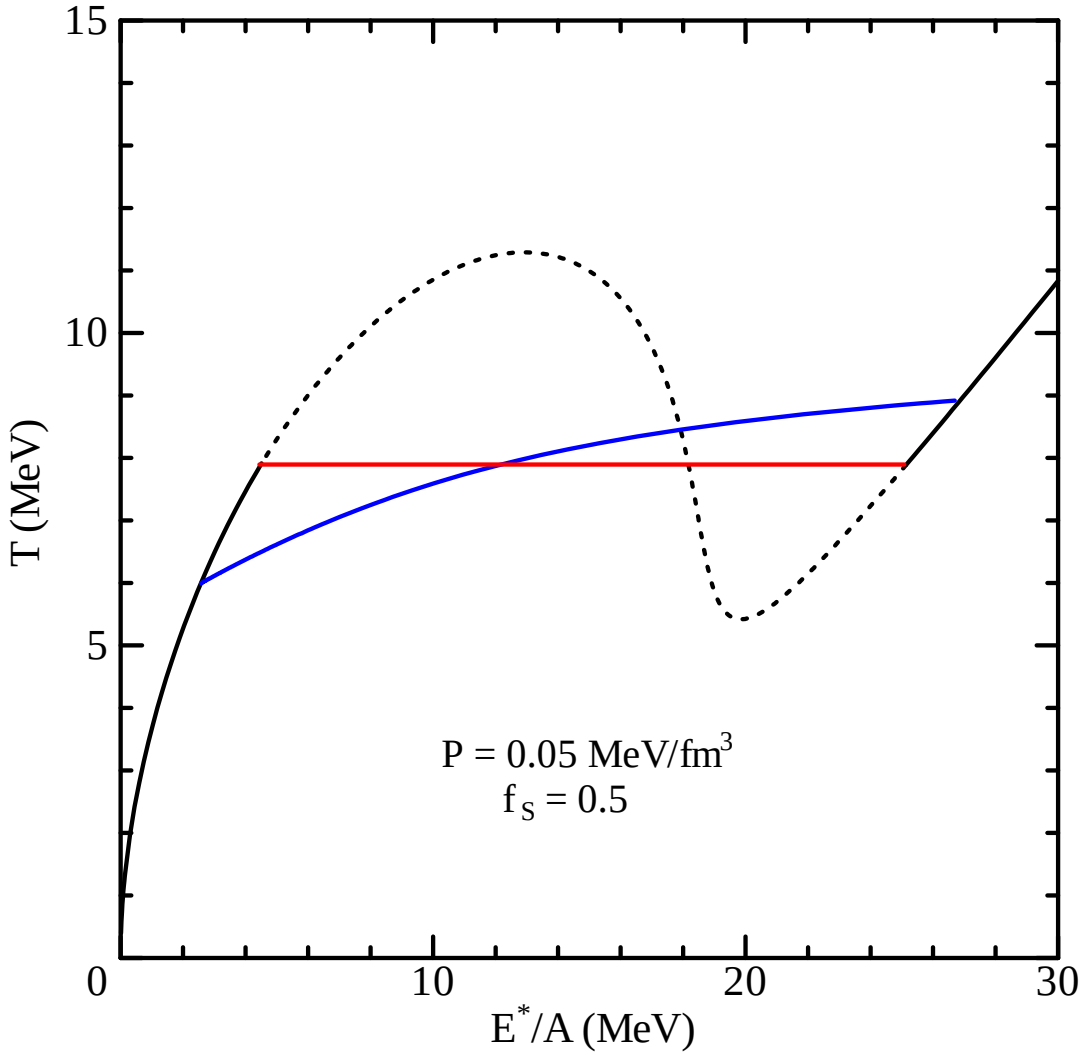

Figure 9: The black curve is the caloric curve derived from the black curve in Fig. 7. The horizontal red line is the boiling temperature in liquid-gas phase transition from the common tangent in Fig. 7. The blue curve is the caloric curve in the phase transition derived from the blue dashed curve in Fig. 7.

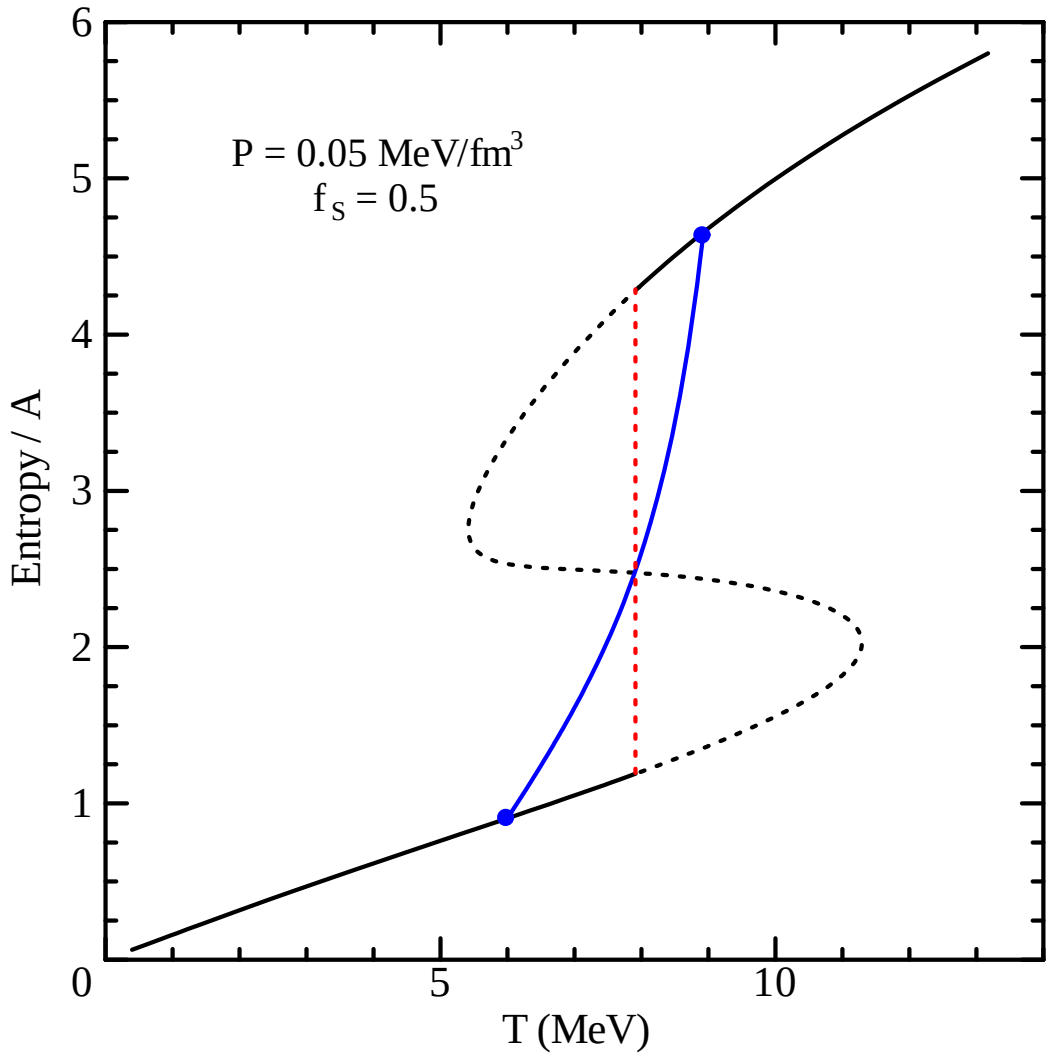

Figure 10: The entropy par baryon as a function of temperature. The black dotted curve is the result in a region of the convex in Fig. 7 and so is not realized. Consequently, the black solid curve exposes a discontinuity marked by the vertical red dotted line. The blue curve is the entropy in liquid-gas phase transition, which satisfies the Gibbs condition on phase equilibrium.

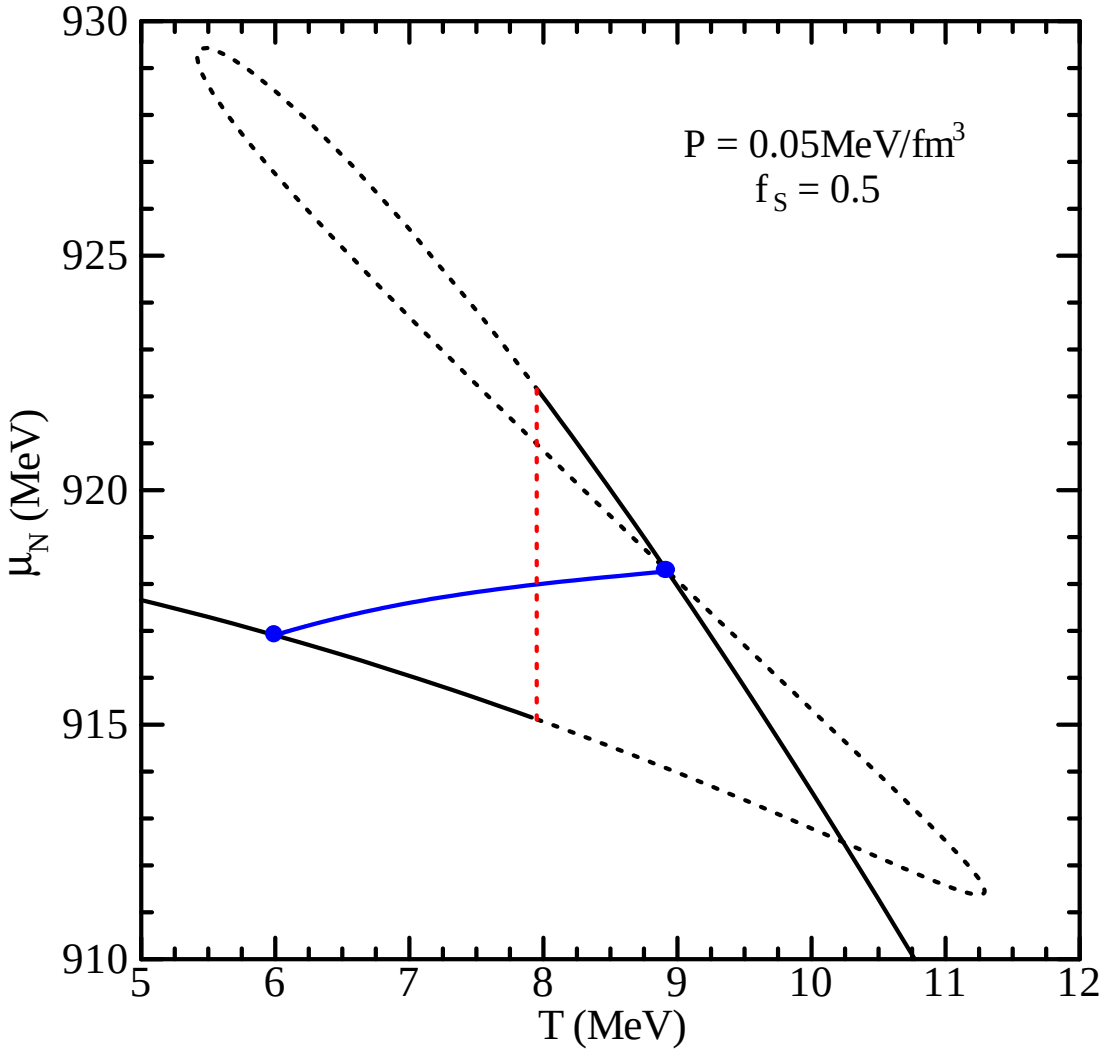

Figure 11: The chemical potential of nucleon as a function of temperature. The black dotted curve is the result in a region of the convex in Fig. 7 and so is not realized. Consequently, the black solid curve exposes a discontinuity marked by the vertical red dotted line. The blue curve is the chemical potential in liquid-gas phase transition, which satisfies the Gibbs condition on phase equilibrium.

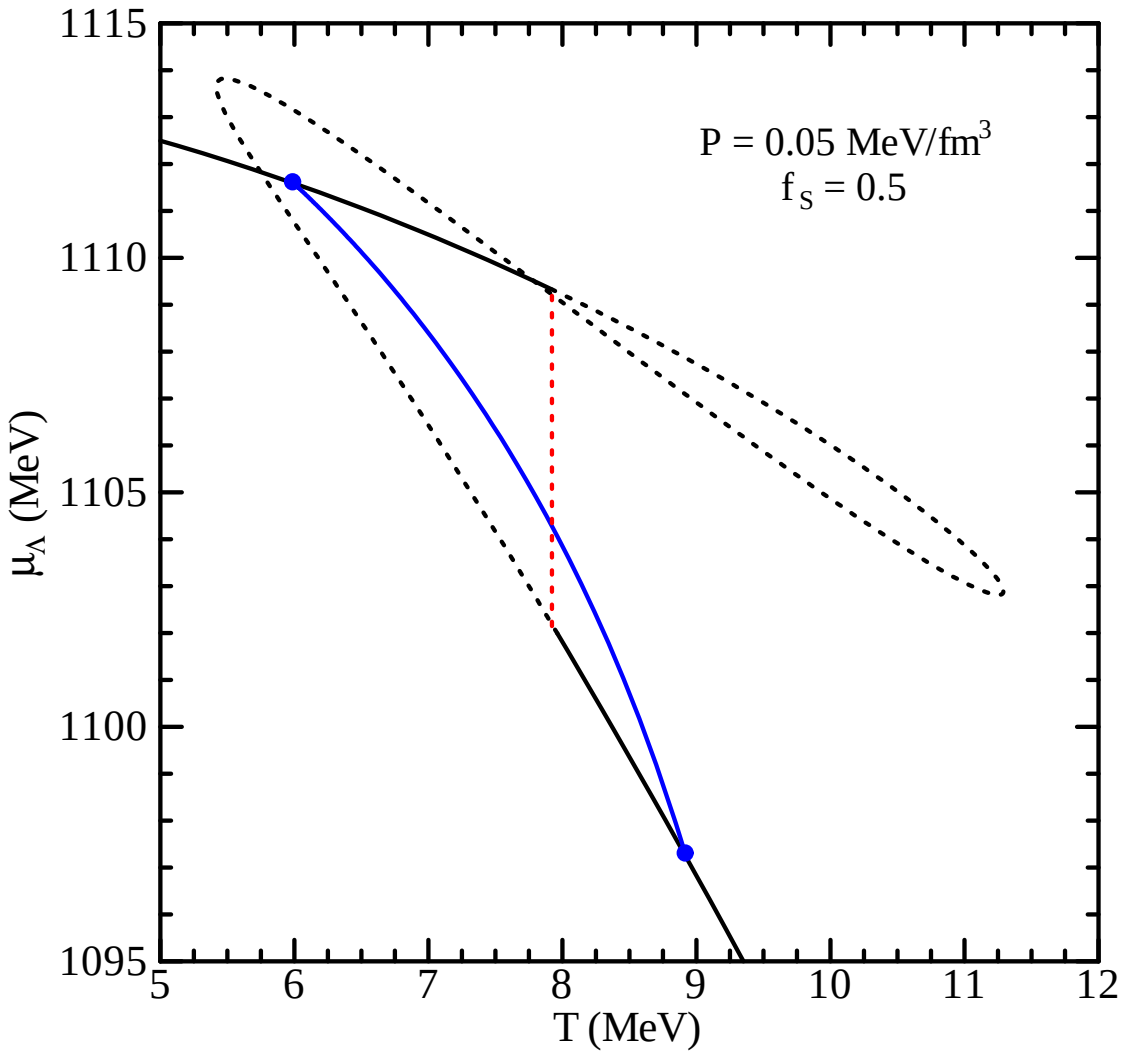

Figure 12: The same as Fig. 11 but for μ_Λ.

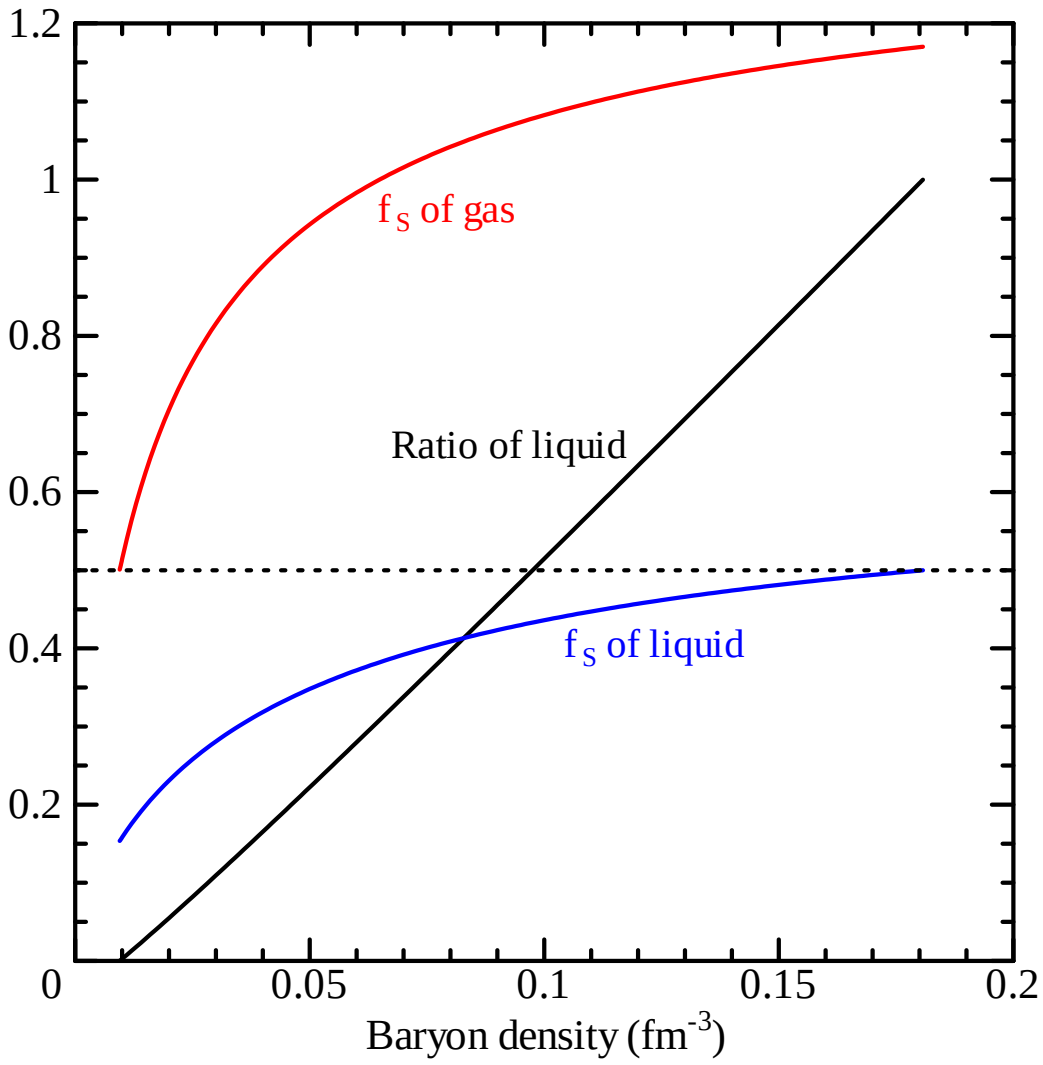

Figure 13: The black curve is the ratio of liquid $f_l = 1 - f_g$ as a function of the total baryon density in the phase transition between $\rho_T = 0.01\text{fm}^{-3}$ and 0.181fm^{-3}. The red and blue curves are the strangeness fractions of gas and liquid, $f_S^{(g)}$ and $f_S^{(l)}$, in Eq. (27).

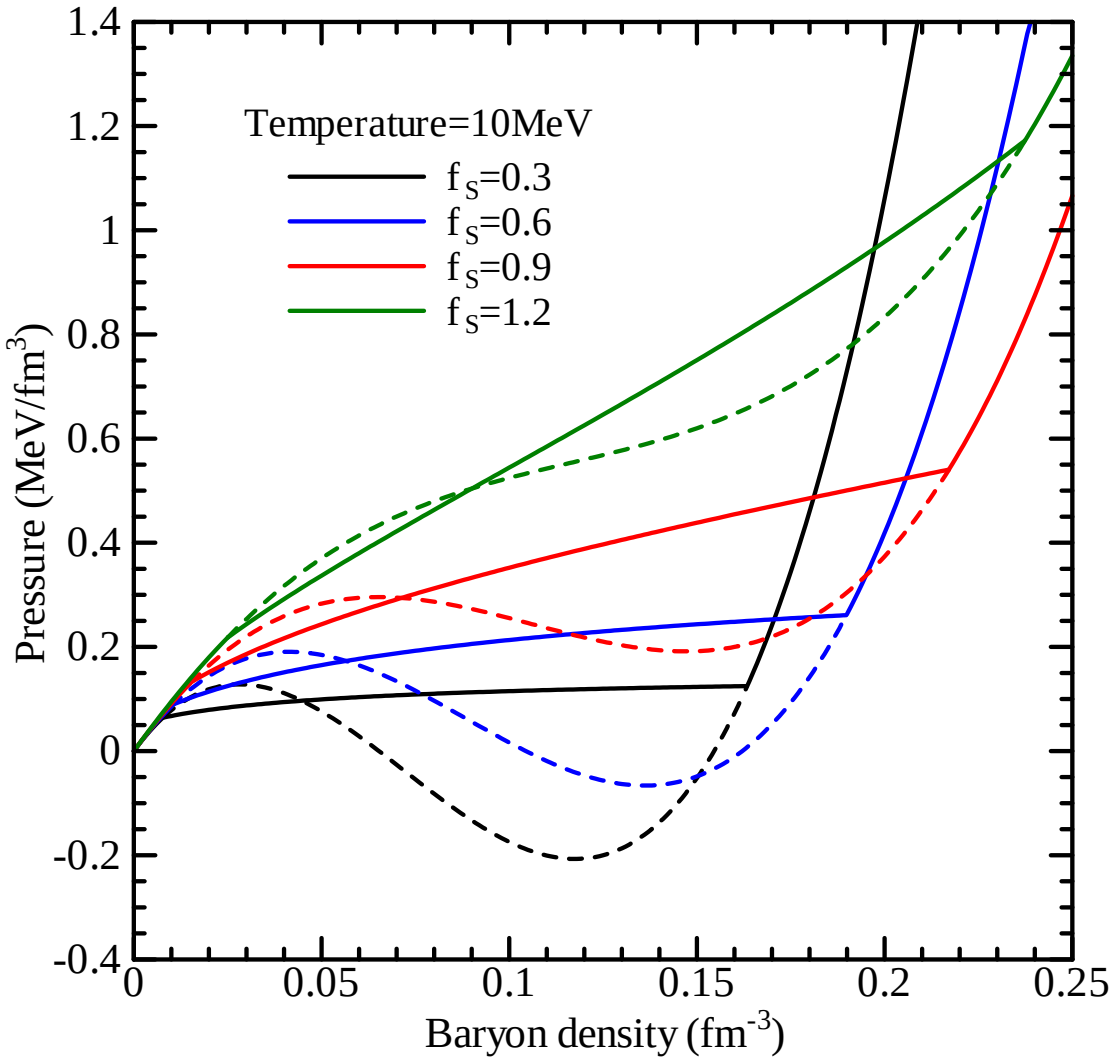

Figure 14: The pressure-density isotherms of $T = 10$MeV for strangeness fractions from $f_S = 0.3$ to $f_S = 1.2$. The solid curves from Eq. (30) are realized while the dashed curves from Eq. (15) are spurious.

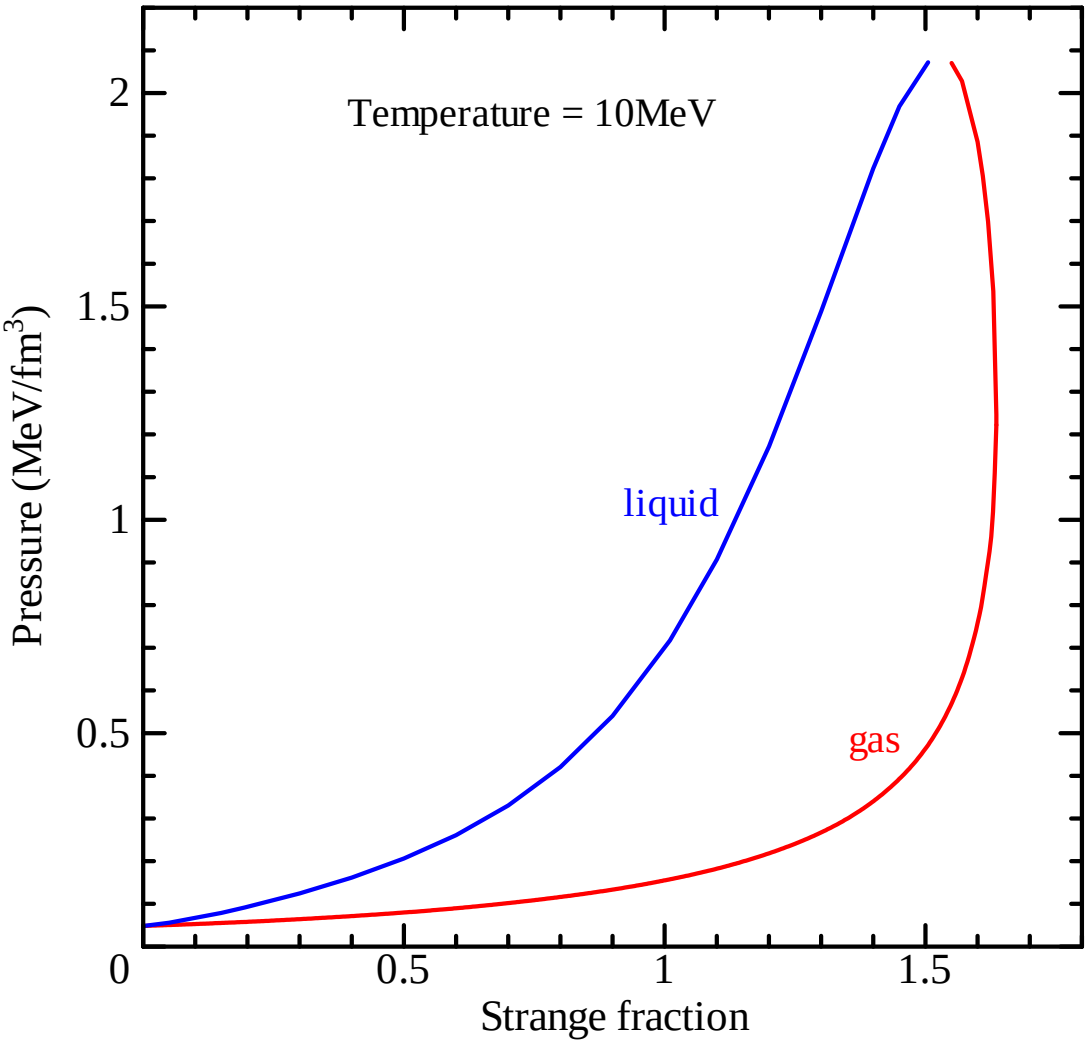

Figure 15: The section of binodal surface at $T = 10$MeV.

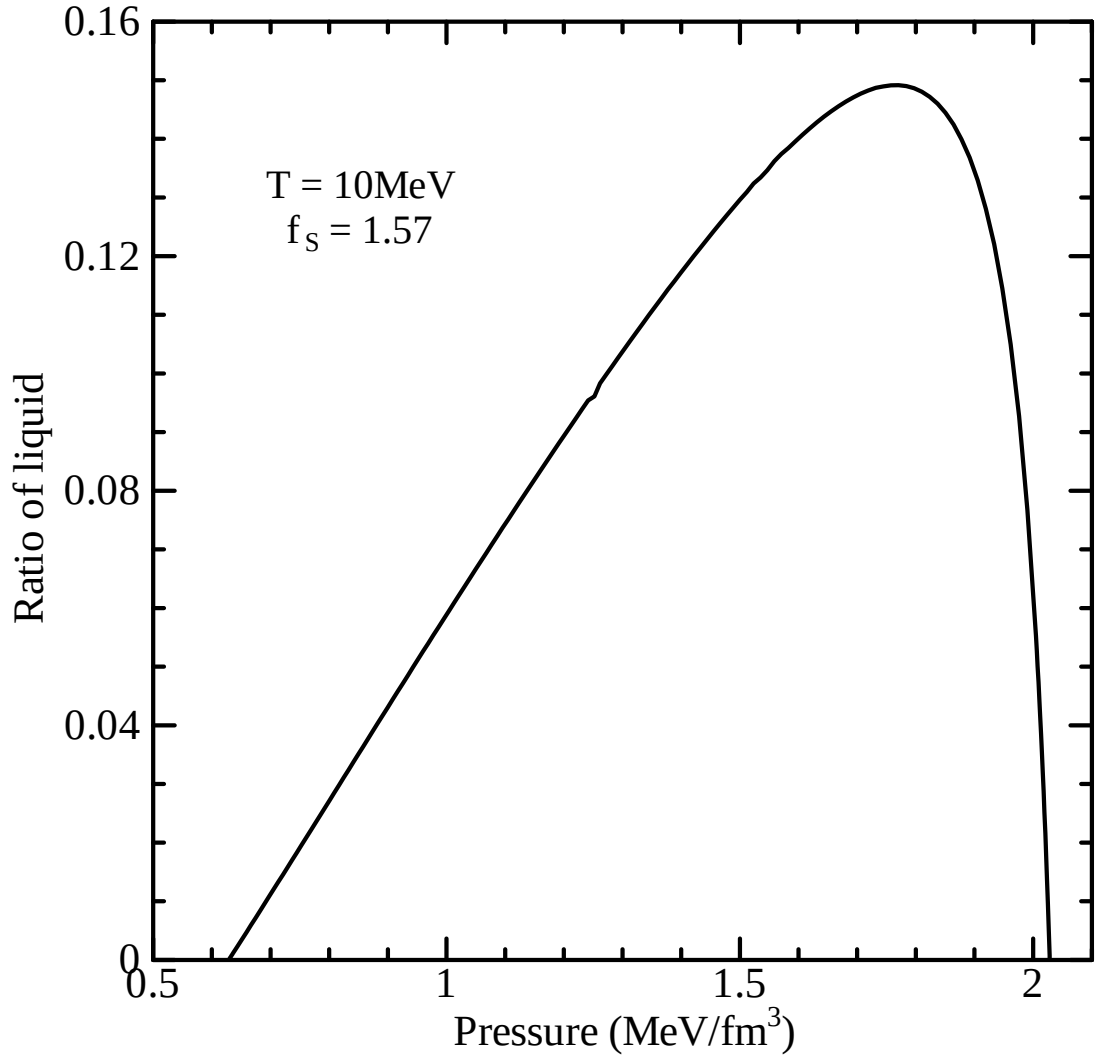

Figure 16: The ratio of liquid as a function of pressure for strangeness fraction $f_S = 1.57$ at $T = 10$MeV.

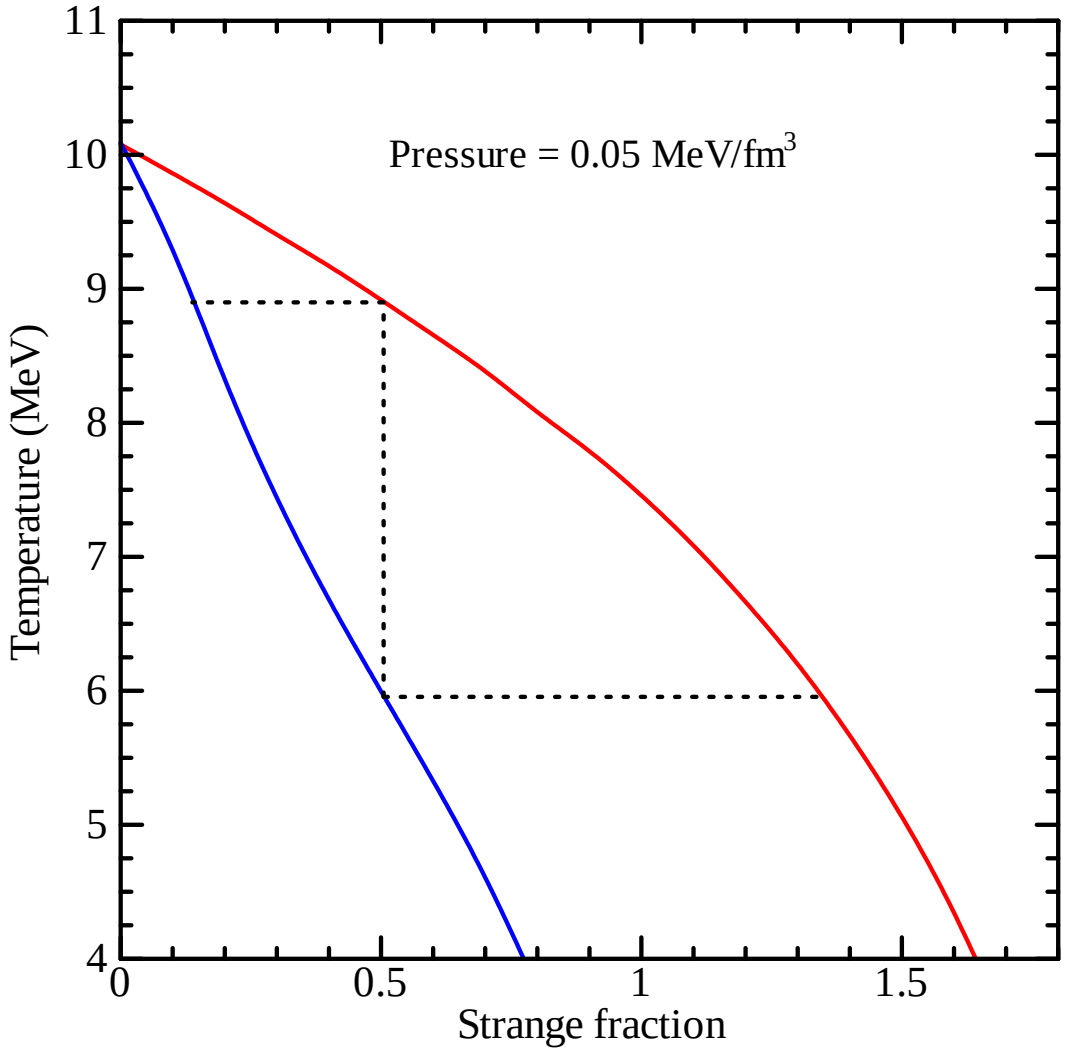

Figure 17: The boiling (blue) and condensed (red) curves of nuclear liquid and gas under the constant pressure $P = 0.05\text{MeV/fm}^3$. The dashed line show the boiling process in SHM liquid of strangeness fraction $f_S = 0.5$.